Spring 6-15-2023

Additive Manufacturing of Stretchable Strain Sensors: Fabrication, Optimization and Application

John Nady Shihat Bastawrous
joo.nady@aucegypt.edu

THE AMERICAN UNIVERSITY IN CAIRO
الجامعة الأمريكية بالقاهرة

School of Sciences and Engineering

Additive Manufacturing of stretchable strain sensor: fabrication optimization and application

A THESIS SUBMITTED BY

John Nady Shihat Bastawrous

TO THE

Nanotechnology Department

in partial fulfillment of the requirements for the degree of

The Master of Science in Nanotechnology

Declaration of Authorship

I, John Nady Shihat Bastawrous, declare that this thesis titled, "Additive Manufacturing of stretchable strain sensor: fabrication optimization and application" and the work presented in it are my own. I confirm that:

- This work was done wholly or mainly while in candidature for a research degree at this University.
- Where any part of this thesis has previously been submitted for a degree or any other qualification at this University or any other institution, this has been clearly stated.
- Where I have consulted the published work of others, this is always clearly attributed.
- Where I have quoted from the work of others, the source is always given. With the exception of such quotations, this thesis is entirely my own work.
- I have acknowledged all main sources of help.
- Where the thesis is based on work done by myself jointly with others, I have made clear exactly what was done by others and what I have contributed myself.

Signed: John Nady Shihat Bastawrous

Date: 7/2/2023

Abstract

In this project, a novel strain sensor design is fabricated employing different additive manufacturing techniques. The spring sensor's primary material is PLA-Like resin with a nanocomposite encapsulation layer as the functional material. The main principle of Straining the sensors results in a change in resistivity as the distances among the conductive carbon particles change according to the strain applied.

Sensor fabrication consists of two parts: spring manufacturing and development of nanocomposite encapsulation The nanocomposite matrix is developed through the dispersion of Graphene and Carbon nanotubes in Th**e**rmoplastic Polyurethane through sonication and magnetic hotplate stirring. While the spring itself is manufactured by injection molding, the spring is dip-coated in the TPU-Carbon nanocomposite to fully develop the functional spring sensor.

The novel sensor design, nanocomposite development, and fabrication processes optimization combine to maximize key performance indicators which are: high gauge factors and large extension percentages. This project reports a maximum gauge factor of 950 and an extension of 300% of the initial sensor length. These promising electrotechnical properties show great potential to be employed in numerous applications, in this report, respiration monitoring for preterm infants is discussed as the main challenge to be addressed. Wearable sensors for infant respiration monitoring face some challenges with low gauge factors and stretchability. The application of this sensor addresses the current problems in the electromechanical behavior of current wearable systems reported in the literature.

Acknowledgments

This work would have not been completed without the guidance of Dr. Mohamed Serry and the help of my colleagues Mohammed Waheed and Khaled Al-Toukhy.

Contents

List of Figures

List of Tables

List of Abbreviations

AM	**Additive Manufacturing**
GF	**Gauge Factor**
MWCNT	**Multi-Walled Carbon Nanotubes**
PLA	**Polylactic acid**
DMF	**Dimethylformamide**
TPU	**Thermoplastic Polyurethane**

List of Symbols

G	*Shear modulus of the spring main material*
K	*Spring constant given the spring geometry and material*
C	*Ratio of Mean Diameter to Wire Diameter*
W	*Wahl's Correction Factor*
δ	*Linear deflection*
γ	*Torsional Strain Resulting from spring deflection*
τ	*Shear Stress*
D	*Diameter of Spring (Mean)*
d	*Wire Diameter of the Spring*

Chapter 1

A New Pathway for the Additive Manufacturing of Nanocomposite Functional Devices

1. Introduction

1.1 Respiration Monitoring:

Quality of human life is a main concern lately in research, by development and fabrication of new wearable sensors technologies and concepts, that fulfill sensitivity, sustainability, and high functionality. Flexible substrates were proposed lately in research to overcome the problem of mobility and flexibility as solid, rigid substrates fabricated by MEMS technique do not provide a larger extension with high GF and functionality, when it comes to strain sensors. Various fabrication techniques can be used in flexible sensors ranging between contact and non-contact printing techniques, including 3D-printing, and inkjet printing, in which polymeric substrates and sensing materials are utilized in the needed functional geometry to perform the objective to the sensor precisely on different size scales. Polymeric composite materials are widely used in those applications as flexible and sensitive materials, which are easily deformed by motion causing a change in the electronic output signal connected to the circuit allowing for real-time motion detection. This electromechanical interaction can be easily utilized in health monitoring applications such as respiratory performance [1,2].

Respiration is a vital health indicator of various pathological conditions that could be physical or mental. Respiration involves multiple structures: lungs, brain, muscles, brain stream, and blood vessels [3]. Any occurrence that affects these structures will influence the

respiration rate.

As the lungs' volume change contractions and expansions occur. Real-time monitoring of respiratory conditions is crucial for handling serious medical emergencies. Identifying respiratory patterns has also provided more insights into numerous medical conditions and accordingly limited their damages. [3,4,5]. Thus, a reliable, robust, and accurate respiratory sensor is of great significance. Respiratory motion is sensitive to stressors and cardiac events of the human body. Respiratory frequency (f_R) monitoring provides important information about the human body's physical and mental conditions.

(f_R) is affected by many factors such as emotional and cognitive stress, hyperthermia, fatigue, and other medical conditions [6]. Real-time monitoring (f_R) provides accurate supervision for both chronic and acute medical conditions. Examples of physical disorders include chronic heart and respiratory diseases such as pneumonia and asthma [7]. (f_R) helps with respiratory muscle assessment and muscle fatigue. This is critical for vulnerable age groups who are at high risk of respiratory muscle problems [8]. For mental health, (f_R) monitoring is helpful for psychological disorders such as panic and anxiety disorders [9].

Supervision over respiratory variability helps with handling unexpected cardiovascular events and provides real-time feedback for immediate medical intervention to limit any casualties. In addition, identifying breathing patterns could predict serious occurrences. Hence, f_R monitoring has limitless potential and could help foresee and treat various medical problems and limit casualties of any sudden medical emergencies [10].

In addition to respiration rate monitoring, the range of motion of the chest area can be measured to provide more information on the amount of oxygen intake and breathing patterns which are critical for patients, especially after the outbreak of the covid-19 virus which attacks the human respiratory system. Moreover, it can help predict and treat further complications and long-term effects of covid-19 [12].

Studies of chest expansion have reported that chest expansion medians around 5 and 4.9 cm for girls, 6 and 5.9 cm for boys, and 5 and 5.6 cm for healthy adults [13]. Other studies have reported a maximum of 8.1 ± 2.5 cm of chest expansion [14]. This range of chest expansion is still within the spring's expansion capability in the elastic region with a margin far away from the spring's plastic deformation extension threshold.

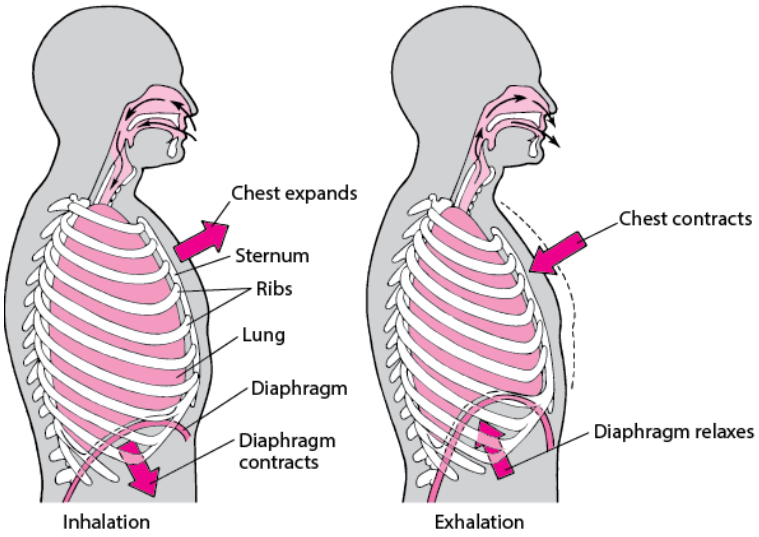

Figure 1 Illustration of Inhale-exhale mechanism [15]

1.1.1 Application of Respiration Monitoring for Preterm Infants and neonates:

Respiration Destress: Observations, Causes, and Complications

Premature or preterm are terms used to identify infants who are born usually before completing 37 weeks in the womb. [16] Due to their early delivery, their organs are often not

fully formed and might not be fully or properly functional which makes them prone to serious medical problems if not provided with professional medical care. Numerous studies are concerned with premature infants to address the main problems they face in their early development stage. Early development stages are critical for organ formation which affects individuals in their lifetime. Statistics show that around 8-10% of all pregnancies are preterm [16], out of which around 2 million babies are extremely preterm as they were delivered < 32 weeks. [17]. Of all preterm deliveries, around 2.9 million babies die in their first 28 days with respiratory disorders being the main fatal mortality cause. [18]

Respiration is critical for the early development of infants as it provides their cells with oxygen to further develop and function. Thus, any deviation in respiratory processes causes damage to other organs. Examples of respiratory problems for preterm infants include respiratory distress syndrome, transient tachypnea, bronchopulmonary dysplasia, pneumonia, neonatal respiratory distress, meconium aspiration, apnea, and pulmonary hypertension. [19]. The abovementioned respiratory diseases and complications could lead to complete respiratory failure if not treated properly.

A key element in the respiratory system is lung surfactant. Lung surfactant has proteins that are vital for respiration. These proteins make this surfactant critical for two main reasons: it lowers the surface tension between air and liquid in the respiratory system to prevent any potential alveolar collapse. Secondly, surfactant modulates and helps the immune response as it kills pathogens due to their antimicrobial properties [20]. Preterm infants usually have deficiencies in surfactant production which makes them prone to subsequent complications. Lack of surfactant is a leading cause of respiratory distress which causes high mortality rates in preterm infants.

Respiration of preterm infants is monitored on both frequency (f_R) and pattern levels. For newborns, f_R ranges between 30 to 60 breaths per minute. Measuring irregularities in respiration is a vital indicator of underlying problems [18,21]. In addition to (f_R), respiratory retraction rate or inhale-exhale movement of the chest and abdomen of an infant is a key indicator of potential respiratory distress. Thus, monitoring breathing depths and patterns is critical for ensuring the healthy development of preterm infants.

Lung or pulmonary compliance refers to the expandability of the infant's lungs, when lung compliance is low, f_R increases to make up for the decrease in the lungs' volume. In some cases, newborns still have fetal lung fluids that weren't cleared which reduces the functionality of their lungs resulting in rapid breathing known as transient tachypnea (TTN). Respiratory distress syndrome (RDS) is another condition that happens when infants don't have enough surfactant to support their lungs' expandability requiring them to breathe at higher (f_R). [22] Respiration is a passive process, when premature infants have respiratory distress, their abdominal muscles get involved to help their breathing. Thus, higher abdominal expansion and involvement indicate possible problems. The following table summarizes causes for respiratory problems for preterm infants as well as non-respiratory problems that could cause respiratory distress. [19]

Preterm pathology	Term pathology	Congenital anomalies/surgical conditions	Non-respiratory causes of respiratory distress
Respiratory distress syndrome	Transient tachypnoea of the newborn	Congenital pulmonary airway malformation	Heart failure (due to congenital heart disease)
Pneumothorax	Respiratory distress syndrome	Congenital diaphragmatic hernia	Neuromuscular disorders
Pneumonia	Meconium aspiration	Tracheo-oesphageal fistula	Hypoxic ischaemic encephalopathy
Pulmonary haemorrhage	Primary or secondary persistent pulmonary hypertension of the newborn	Choanal atresia	Metabolic acidosis (due to inborn error of metabolism)
Aspiration	Pneumonia	Pulmonary sequestration	
Pleural effusion (chylothorax)	Pneumothorax	Congenital lobar emphysema	
Chronic lung disease	Aspiration		
	Pleural effusion (chylothorax)		
	Pulmonary haemorrhage		
	Surfactant protein deficiency syndromes		
	Alveolar capillary dysplasia		

Table 1 common issues that cause respiratory distress in preterm infants [19]

Since respiration is significantly linked to heart and brain function, respiration rate is also an indicator of cognitive problems. numerous studies have linked irregularities in (f_R) and breathing patterns to possible problems in brain development and cardiovascular functionality. Respiratory problems affect the infant's brain function and development since their brains are not supplied with an adequate amount of oxygen or might trap toxic oxygen. Problems with oxygen supply to the brain might lead to brain tissue damage and inflammations which have incurable or irreversible consequences in the long term. The following diagram illustrates and summarizes the possible complications that could follow due to respiratory problems. At this early stage, brain and heart formation and functionality are hugely dependent on lung efficiency. Complications include cardiovascular problems and immature brain formation and possible brain inflammation. This diagram shows how respiratory distress relates to other brain and heart problems.[23]

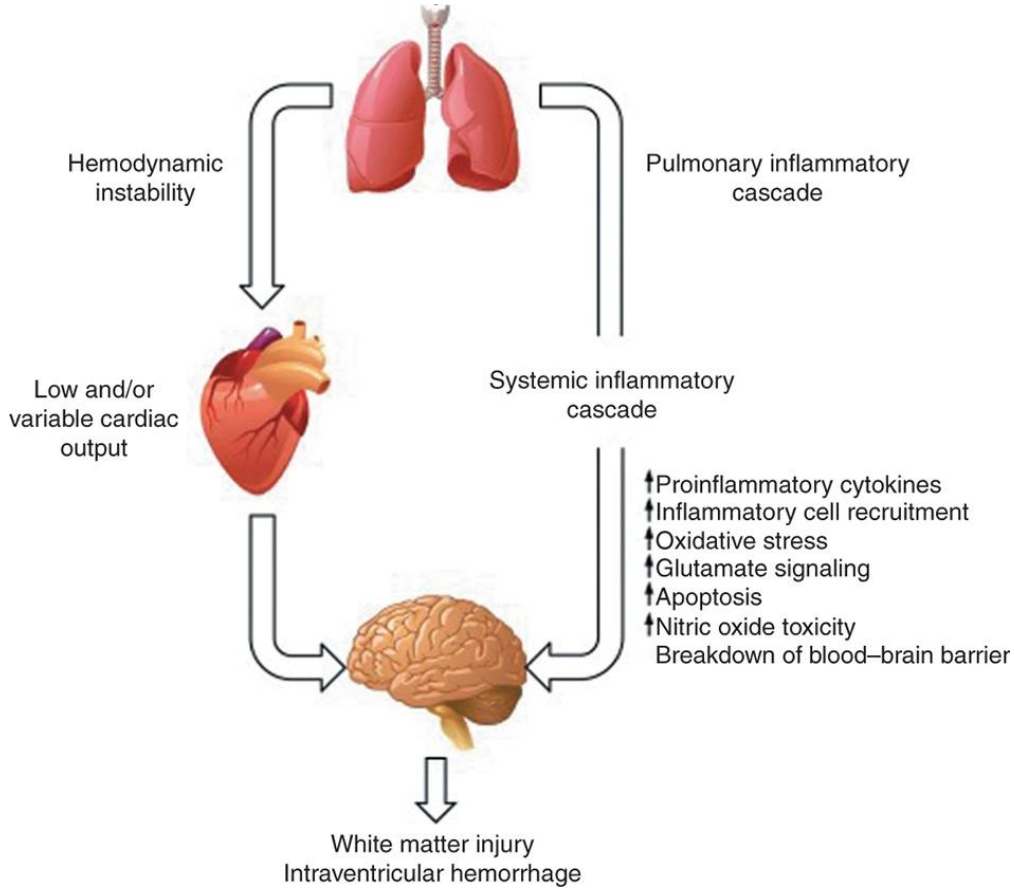

Figure 2 Diagram of possible future complications of respiratory problems in preterm infants [23]

The following table demonstrates how the chest and abdominal retraction alongside respiratory rates are used as indicators of possible failure in the respiratory system [22]

Score	Respiratory rate	Cyanosis	Air entry	Grunt	Retraction
0	<60/min	Nil	Normal	None	Nil
1	60-80/min	In room air	Mild ?	Ausc with stethoscope	Mild
2	>80/min	In >40%	Marked ?	Audible with naked ear	Moderate

A score of >6 is indicative of impending respiratory failure.

Table 2 respiration rate and retraction as indicators for potential respiratory failure [22]

After examining the causes and potential respiratory problems that could be detected and treated by immediate medical intervention. The case is now narrowed down to a case study

in Egypt to highlight the significance of respiratory distress for preterm infants. This study was done in Qena governorate and the following table illustrates the lead causes of respiratory distress (each cause could be identified by a breathing rate and a breathing pattern as abovementioned)

Different causes of neonatal respiratory distress.

Type	Frequency	Percentage(%)
Respiratory distress syndrome	72	49.6%
Transient tachypnea of newborn	32	22.1%
Respiratory distress due to pneumonia	25	17.2%
Meconium aspiration syndrome	9	6.1%
Congenital diaphragmatic hernia	3	2.1
Aspiration of milk	2	1.4%
Tracheosophogeal fistula	2	1.4%
Total	145	100%

Table 3 Respiratory distress causes for preterm infants in Egypt, Qena.[24]

In summary, respiration morbidity and distress could be caused by various health issues in preterm infants, these issues are related to the incomplete formation of their organs which affects their functionality. Health issues in preterm infants cause identifiable irregularities in their respiration rate and chest/abdominal retraction levels. Numerous studies have proven that respiratory distress causes high mortality rates for preterm infants. Respiratory issues are problematic for the child's development both in the physical and cognitive aspects and in the long term they could cause incurable damages if not treated properly at an early stage. While keeping a close eye on the health condition of infants is critical to prevent any foreseeable failures.

1.1.2 Advancements in Respiration Monitoring:

After highlighting how critical respiration monitoring is for preterm infants, in this section, current advancements in respiration monitoring for premature infants include will be examined in detail to highlight the pros and cons of these systems. Respiration monitoring systems could be categorized into categories: monitoring through systems physically attached to the body, and contactless systems that observe and analyze the physical state of the baby through monitors.

1.1.2.1 Contactless monitoring systems:

Non-contact systems and radar sensors are often used to analyze and detect motion. There are camera-based monitoring and radar monitoring systems. Radar monitoring systems usually send electromagnetic waves and are based on the measurement of changes in the waves, motion could be detected. Examples of radar monitoring systems are infrared monitoring and Doppler radar systems. Another popular radar technique is frequency-modulated continuous wave (FMCW). For radar techniques, machine learning models are incorporated into the system. A machine learning model extracts features and then classifies the case based on the breathing characteristics and patterns to draw useful conclusions about the current physical state of the patient. [25]

Camera-based monitoring systems rely on image processing and analysis as an algorithm is employed to analyze the images captured through the camera. An example is optoelectronic plethysmography which monitors movements by observing reflective points on the chest and abdomen. [26] Like radar systems, machine learning models are used to extract features from captured images and then classify or regress to evaluate the current physical state.

Non-contact monitoring systems are greatly affected by the model or algorithm used to process their measurements; their accuracy is deeply dependent on model efficiency. Thus,

numerous monitoring systems are still being researched to address the shortcomings of the abovementioned systems, more research is concerned with developing a more robust model that is not volatile to change.

1.1.2.2 Wearable sensors as monitoring systems:

Wearable sensors are devices that get attached to the body to measure a certain physical characteristic. Respiratory effort belt transducer (REBT) is a belt that is worn around the chest that measures the diameter of the chest as expands and retracts. Other sensors are spirometers, respiratory inductive plethysmography, and piezoelectric transducers.

Wearable sensors or attachable monitoring systems have some drawbacks, for continuous monitoring, the system is usually bulky in the case of preterm infants, and it might hinder their breathing and movement in the case of continuous monitoring which could cause distress to preterm infants. Gauge factors are the change of resistance per strain applied, smaller systems have lower gauge factors due to their size and material restrictions. In literature, Gauge factors below 3 are reported in stretchable strain sensors with stretchability reaching around 200%. [27]

Other wearable sensors in literature are only reporting breathing rate and not breathing depth or volume which is a key characteristic in respiration monitoring.

Perfusion is defined as the blood flow rate through blood vessels in the tissues. This blood flow could be disturbed locally at the contact surface between the skin and the sensor. Thus, if this flow is interrupted due to external factors or is internally disturbed for some reason, it could lead to inaccurate measurements which is a problem with contact and wearable devices. The proposed mechanism is more robust compared to other wearable or attachable sensors in this regard due to the novel design which lowers contact area with the skin.

The sensor's novel design has a lower contact area with the skin which minimizes any potential of measurement errors caused by deviations in skin perfusion. Moreover, the measurement is dependent on the strain induced by the inhale-exhale movements which provides better and more accurate measurement of the breathing pattern, rate, and respiratory range.

1.2 Nanocomposite Sensors and Devices:

Nanocomposite devices have a wide range of functionalities due to the integration of nanofillers and nanodevices which caused a breakthrough in device performance and functionality. Thus, various methods are developed to fabricate nanocomposite devices. Fabrication techniques include gas foaming, melt mixing, electrospinning, sonication, and in-situ polymerization. [28]

AM adds the advantage of fabricating complex designs that could be more functional. In the novel sensor design, the sensor is a spring. The advantage of this spring design is enhanced mechanical properties, reaching for 300% extension, and reduced contact area. These properties are critical for the sensor functionality which will be discussed in detail in the coming sections. Such a complex design could be achieved by AM and injection molding. Given its clear advantage of achieving design complexities with high accuracy, AM fabrication of functional devices still has some limitations. AM fabrication is limited by material options, dimensional accuracy for extremely small details, long run times, and scalability.

Conductive polymeric sensors have been the focus of a lot of research due to their unique property of being flexible and conductive. The need to develop flexible sensors was the main driving force for research to explore the uses of these conductive polymeric materials. Usually, conductive polymeric materials involve the use of a conductive material, for signal collection, and a polymeric flexible material, to act as the insulating matrix. Carbon-based materials, such as Carbon Black, Graphene, and Carbon Nanotubes (CNTs), are among the most common conductive material used for signal collection. Each type has its own advantages where graphene provides a better and cleaner signal compared to carbon black but, in turn, it is harder and more expensive to fabricate and produce [29] Carbon materials are conductive,

when separated and not in direct contact, a potential barrier is created. Due to the dual nature of electrons, the wave behavior of electrons allows for electron tunneling and passing through the high potential barrier. [30].

Two important parameters in obtaining a consistent and clear signal are the weight fraction and dispersion of the carbon material within the matrix. Weight percentages are important as too much or too little of the carbon material could affect the resistivity of the entire system since the overall resistivity of the composite is a function of both the weights and the resistivity of the constituents [31]. Furthermore, too much carbon would result in bad sensitivity as there would be a lot of carbon particles within, and during the strain values required for the application, no change in resistivity will be noticed due to the carbon particles being relatively close. Also, a good dispersion of carbon in the matrix is needed to ensure that there is no agglomeration within the length of the matrix. Agglomerations would cause inconsistent readings when collecting signals across the length of the sensor due to the high concentration of carbon in one region compared to the other regions [32].

Chapter 2

Methodology: System concept and Fabrication

2.1 Principle of operation

2.1.1 Spring Design and Dynamics

Spring concept and working mechanism are illustrated to explain how the novel design works. The motivation behind this sensor spring design is to address the shortcomings of current monitoring techniques. As explained in the literature review, textile wearable sensors that are reported in the literature have some problems with limited stretchability, the comfort of use when worn by preterm infants, the accuracy of monitoring which is affected by local skin perfusion, skin irritation, and most importantly the sensor's gauge factor. Textile wearable sensors reported GFs below 10. Thus, the motivation of this spring design is to minimize skin irritation and be robust against skin perfusion by minimizing the contact area between the spring sensor and the skin.

The application of the novel sensor could be through mounting the spring sensor on a strap around the abdomen or chest to without direct contact with the skin. In this way, the spring sensor will deform according to the breathing pattern and depth of the infant.

GF is defined as the ratio of relative change in electronic resistivity to strain or fractional change in length.

$$GF = \frac{\Delta R/R}{\varepsilon} \quad (1)$$

For this spring design, there are two types of strain: linear or longitudinal strain when the spring is extended or retracted and torsional strain when the torsion is applied to the encapsulation layer due to extension-retraction movements.

The GF is a key parameter for better electromechanical sensor performance. Thus, a considerable amount of the work on this project is intended to maximize the GF. Increasing the GF is optimized through fine-tuning the filler material ratio in the encapsulation layer to result in the maximum possible change in resistivity with respect to the strain applied. The encapsulation nanocomposite layer contains conductive carbon particles. Carbon particles are dispersed into the Thermoplastic Polyurethane layer. When the spring sensor is stretched, the distances among the carbon particles change, accordingly, the resistivity of the encapsulation layer changes. As the distances change among the particles, the electron tunneling effect also changes accordingly which affects the resistivity of the sensor. Thus, the amount of carbon particles in the TPU base layer is a key factor in determining the sensor's electronic behavior.

The mechanical behavior of the spring also contributes to maximizing the GF. For instance, decreasing the amount of strain required to have a significant change in

resistance which also increases the GF. Hence, there is great emphasis on process optimization, spring design, and material selection to come up with the best selections for enhanced mechanical properties.

Now that the main principle of operation is defined, more key concepts are defined before getting into calculations of the spring dynamics. Spring strain is defined as extension or compression applied to deform the spring of its natural state. The gauge factor of the spring is the ratio of change in resistance to change in length or strain applied. Elastic modulus is the spring's resistance to being elastically deformed, elastic deformation means the spring will retain its initial condition when stress is applied. Resistance of the encapsulating layer defines the conductivity of the layer due to the presence of carbon filler material in the polymer.

Regarding the GF and extension calculations, GF calculations since it's mainly dependent on the encapsulating nano-composite and the distance among carbon particles. Since the change in the layer's cross-section due to strain is extremely small (the layer thickness itself is around 0.15 mm) It is assumed that an increase in resistance due to a decrease in the cross-sectional area of an encapsulating layer is not relevant.

Then we could calculate the expected extension percentage through K (spring stiffness) and G (shear modulus).

Another key characteristic of the sensor performance is torsional strain due to the linear extension applied. As the spring is stretched or compressed and due to the spring geometry, this linear movement translated to torsional strain on the encapsulation layer. Thus, torsional strain is applied to disorient the conductive

particles that exist in the polymeric layer. The following model [33,34] will be utilized and further explained in detail in the results chapter to demonstrate how torsional strain relates to changes in sensor electronic behavior.

$$k = \frac{Gd^4}{8D^3 n_a} \tag{2}$$

$$G = \frac{E}{2(1+\nu)} \tag{3}$$

$$\tau_{max} = \frac{8WD}{\pi d^3} F_{max} \tag{4}$$

$$F_{max} = K\left(L_{free} - L_{solid}\right) \tag{5}$$

$$W = \frac{4C-1}{4C-4} + \frac{0.615}{C} \tag{6}$$

$$C = \frac{D}{d} \tag{7}$$

$$\gamma = \frac{\tau}{G} = \frac{8 * W * D * K * \delta}{G * \pi * d^3} \tag{8}$$

$$\gamma_{max} = \frac{\tau}{G} = \frac{8 * W * D * K * \delta_{max}}{G * \pi * d^3} \tag{9}$$

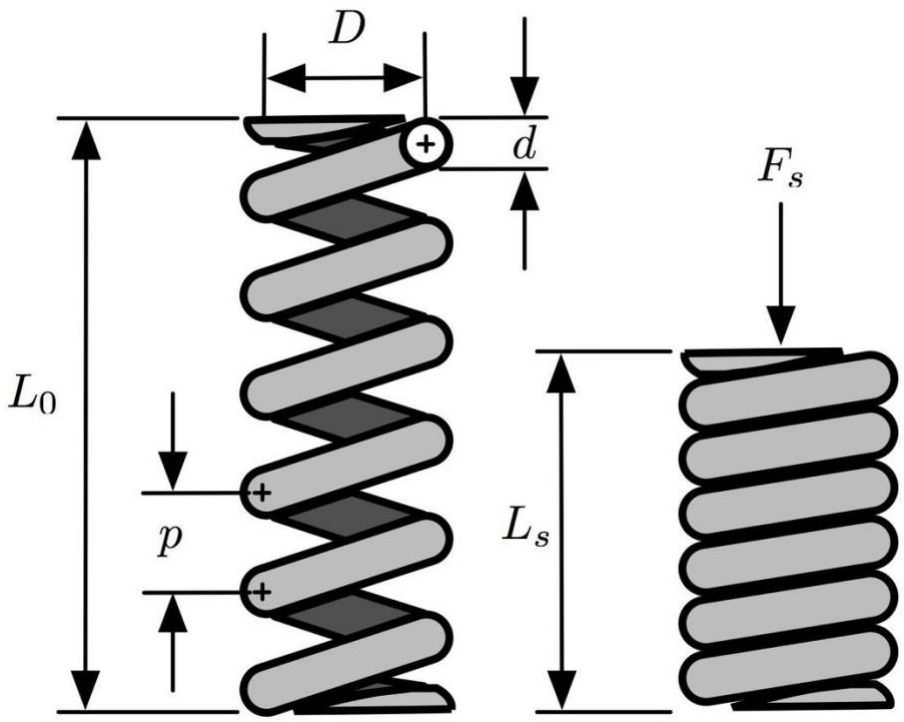

Figure 3 Geometry of spring [35]

2.1.2 Nanocomposite Encapsulation Design:

2.1.2.1 Percolation Threshold in Nanocomposites:

Consider a random system, to establish a connection throughout this system, a long-range connection, percolation threshold must be satisfied. The percolation threshold is defined as the minimum for establishing a connection in a random system. Below the percolation threshold, there is no connection as conductive particles are far away from each other to allow electron tunneling.

Percolation in nanocomposites is a critical parameter in the fabrication process. The percolation threshold defines the minimum weight or volume fraction of nanomaterials present in the matrix which forms a network that allows electron tunneling and causes current to flow through the composite matrix. Thus, the polymer carbon composite becomes

conductive. [36]

Percolation has 3 phases, the first phase is below the threshold where resistance is high, and there is no path or network for electrons to flow through tunneling in the polymer. The second phase is within the percolation threshold or range, where conductivity is starting to be established through random connections throughout the nanocomposite matrix. Within this percolation threshold conductivity is not the highest as conductivity is still restricted to a few random paths as established connections. Therefore, optimization at the percolation threshold area is critical for a good accurate sensor response which will be further explained in the coming section.

The third phase is beyond the percolation threshold the critical percolation threshold area where the network is constructed, and electrons could tunnel and flow through the composite as there are multiple paths for electrons to flow through with more conductive carbon material added. At this point, conductivity is increased which affects sensitivity to change applied. Electron tunneling occurs when there are conductive particles nearing each other with high a resistance barrier in between, electron wave nature causes electrons to bypass these high potential barriers resulting in electron flow. Stress as stimuli causes a change to electronic tunneling behavior as the orientation of host material changes causing changes in orientation among the filler material with higher barriers potentially introduced and affecting electron tunneling behavior. [36, 37]

2.1.2.2 Optimization of Percolation Threshold:

The polymeric spring is made of a Polylactic Acid (PLA)- like resin which is coated with a matrix layer of TPU/Carbon. When an axial force is exerted to extend or strain the spring along its axis, the coat layers stretched as well. Essential at rest, the TPU/Carbon layer (specifically at the percolation threshold) has an established random connection

throughout the layer along the spring. When the spring is axially stretched (Ex: in the exhale movement) the outer layer is also stretched. The strain induced by the exhale-inhale mechanism is transferred to the nanocomposite encapsulation as it is bonded to the spring material through thermal treatment and ultraviolet curing. Due to bonding or adhesion between both layers, the strain is transferred to the encapsulating layer. This expansion in the polymeric layer leads to the increased distance among the carbon particles. At rest, carbon particles are still in their fixed position, while the spring is horizontally strained, and the TPU base layer is stretched which increases the distance among the carbon particles. as a result, the established random connection throughout the nanocomposite encapsulation is affected. This results in higher resistance and barriers for electrons with more difficulties for electron flow and electron tunneling through high resistance barriers. As these barrier increases, the electron flow and tunneling decreases, and resistance increase with strain. This applied strain leads to a significant change in resistance because exactly at the percolation point, there is only one random shortest path for electrons to flow, and this unique connection is greatly influenced by TPU layer extension and retraction.

In the case of high carbon composition in the TPU/Carbon matrix beyond the percolation threshold, there are multiple random paths for electrons to flow throughout the encapsulating layer. Therefore, when the encapsulation layer is stretched, the distances among the carbon particles increase accordingly. However, due to the high carbon composition in the encapsulation layer, there are exists where multiple random connections or paths throughout the TPU/Carbon nanocomposite. These multiple random connections are affected by strain, but still, new paths could be discovered by electrons to path through the layer which is manifested in an increase in resistance but not as critical compared to percolation threshold composition.

In the case of the carbon composition lower than the percolation threshold, at rest, there is no established connection among the conductive carbon particles embedded into TPU.

Therefore, when stretched, the distances among the carbon particles are even multiplied and it becomes impossible for a connection to be established across the encapsulation layer. Thus, it is evident that exactly at the percolation point, the change of resistance per unit strain is at its absolute maximum. Since Gauge Factor is defined as the change in resistance per unit strain, GF is at its peak when TPU/Carbon composition is optimized precisely at the percolation threshold.

As a result, optimization of the TPU/Carbon composition is critical for high GF. The percolation threshold is dependent upon the size and nature of the nanoparticles and the characteristics of the polymer. This project successfully optimizes TPU/MWCNTs and TPU/Graphene composition around the percolation threshold for gauge factor optimization. The following figure illustrates the dynamics between resistivity and percolation threshold.

As a result, optimization of the TPU/Carbon composition is critical for high GF. The percolation threshold is dependent upon the size and nature of the nanoparticles and the characteristics of the polymer. This project successfully optimizes TPU/MWCNTs and TPU/Graphene composition around the percolation threshold for gauge factor optimization. The following figure illustrates the dynamics between resistivity and percolation threshold.

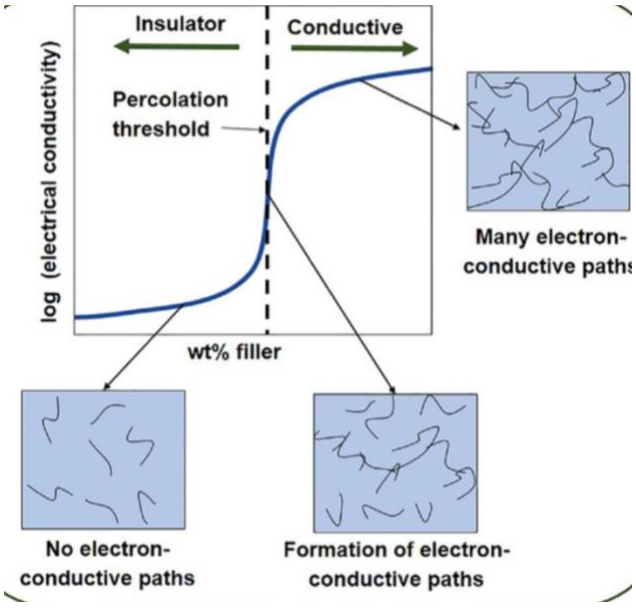

Figure 4 conductivity regions vs weight percentage of fillers [36]

The percolation threshold area is illustrated exactly at the point where the formation of electron conductive paths starts to formulate. Beyond the percolation threshold, many conductive paths exist yielding better overall conductivity.

2.2 Materials and Methods

In this section, all the fabrication processes will be discussed in detail with the motivation behind each step. The fabrication process of the sensor platform was designed and optimized with electrical and mechanical standpoints and the results are discussed in the context of mechanical characterization. This sensor mainly depends on electromechanical coupling in response to applied strain, which is achieved by the concept of tunneling among neighboring carbon-based flakes. This concept was selected mainly for its higher strain sensitivity in comparison with the mentioned techniques in literature, which is attributed to the drastic change in resistivity of the used composite when subjected to strain, leading to an increase in distance between neighboring carbon nanotubes.

This work aims to fabricate a strain sensor designed for high-extension applications such as respiratory monitoring. Spring-based sensors are fabricated through a process of resin injection and UV curing into 3D-printed molds. Fabricated springs are then coated with thermoplastic polyurethane carbon black TPU/CB or TPU/CNTs composite layer for signal collection upon generated straining as shown in Fig.1, which allows for relative displacement of CB particles causing an increase in materials resistivity. The following table summarizes the materials used in the spring sensor fabrication.

Material	Vendor
Mutli-Walled Carbon Nanotubes MWCNTs	Egyptian Petroleum Research Institute
Graphene	AUC Chemistry Department
TPU (Thermoplastic Polyurethane)	Amazon
PLA like resin (clear resin)	Pro Shape

Table 4 Summary of materials in this project

2.2.1 Spring fabrication:

This spring design is fabricated with injection molding. The injection molding process starts with mold design, material selection, and fabrication. The mold design is adjusted according to the desired spring geometry and dimensions. The mold material is selected to satisfy two critical conditions which are: flexibility and transparency. Transparency of mold is critical for curing and solidification of the spring. The mold assembly with spring material injected is subjected to ultraviolet rays to cure the spring material. Therefore, transparency of the mold is critical to let ultraviolet rays into the assembly. As the ultraviolet light goes through the transparent mold material, the spring material starts to cure and solidify through cross-linking. Moreover, transparency allows for better monitoring of the injection process to ensure the resin is properly injected with no air bubbles stuck inside.

Mold material is flexible to allow for the air bubbles to escape the mold during the injection process. The mold material is PLA-like resin which is compatible with spring material. Mold is fabricated with Stereolithography (SLA) 3d printing of two mold halves while the core is 3d printed by Fused Deposition Modeling (FDM). The mold consists of 3 parts: upper half, lower half, and inner core. The cavity between the inner core and the mold's inner walls is a spring geometry with a 10 mm outer diameter and 1.5 mm of cross-section. These specified

dimensions of the mold and spring were selected based on multiple trial and error experiments as the mechanical behavior of the spring was tested for different geometries. The following figure 4 illustrates a disassembled view of the mold in which the spring material will be injected.

Parameter	Value
Bottom exposure time	11 s
Light off delay	4 s
Exposure time	5.5 s
Lifting distance	5 mm
Motor speed	3 mm/s
Bottom exposure layers	9 layers

Table 5 Parameters used in fabricating the mold.

The following figure 4 illustrates a disassembled view of the mold in which the spring material will be injected.

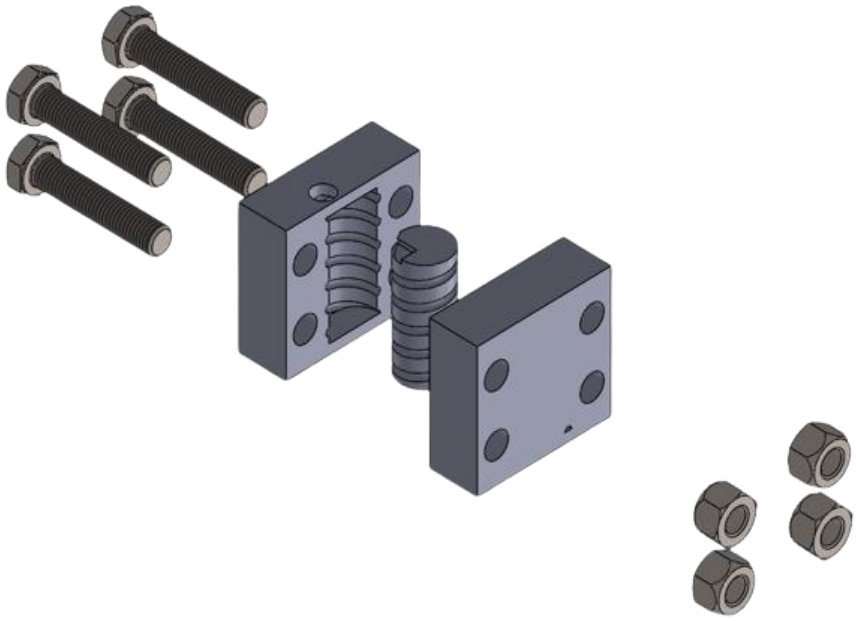

Figure 5 Exploded View of the mold with core, upper and lower halves

Before injection of the spring material, the inner wall and core of the mold are lubricated with silicon-based lubricant for the ease of disassembly and extraction of the spring as it

separates the spring material from both the mold inner walls and core.

Spring material is PLA-like resin, the material is injected into the transparent flexible mold. Resin is injected manually into the assembled mold through an opening at the top. Since the mold is flexible, it allows air bubbles to escape out of the mold. Moreover, the process is easily monitored through transparent mold material. After the injection is done, the mold is exposed to ultraviolet rays for curing. Ultraviolet rays cause crosslinking and solidification of the resin inside the mold. Curing is done for 8 minutes at two different perpendicular orientations to ensure consistent solidification of the spring. The mold is placed around 4 cm from the light source consisting of 18 small sources of UV light (200 mW/cm2) inside the Creality 3d UW-01 Curing Machine. The exposure time was optimized at 8 minutes, 4 minutes for each orientation based on trial and error through examining different curing times and the mechanical properties of the resulting spring.

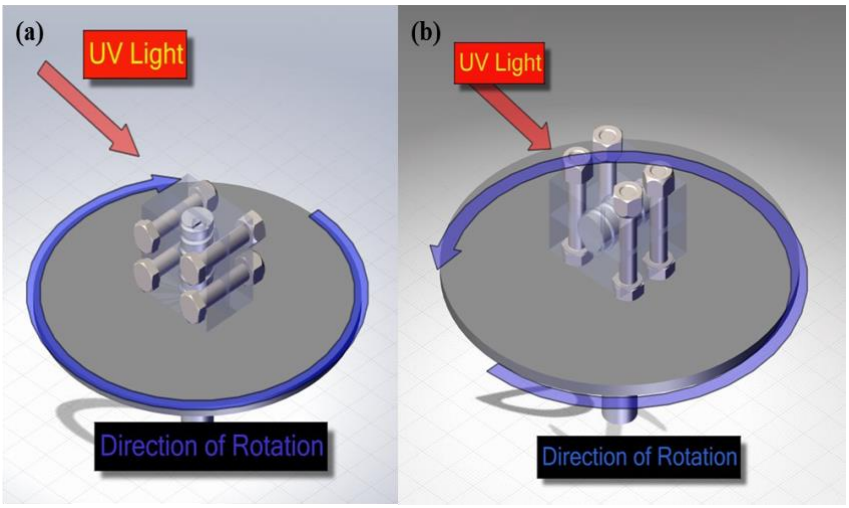

Figure 6 The two steps of curing spring after injection,

(a) First stage of vertical orientation, (b) Second stage of horizontal orientation

Injection molding have proved to be the most suitable for optimizing the spring's mechanical behavior. Other attempts of spring fabrication through direct 3d printing have failed due to two reasons: optimizing the 3d printing process of the complicated structure needed

Furthermore, and there were restrictions on the material selection that could be used with

direct 3d printing techniques which affects the mechanical behavior of the spring. Thus, injection molding has proven to be the most efficient fabrication technique which will be demonstrated later while reporting the mechanical behavior of the spring.

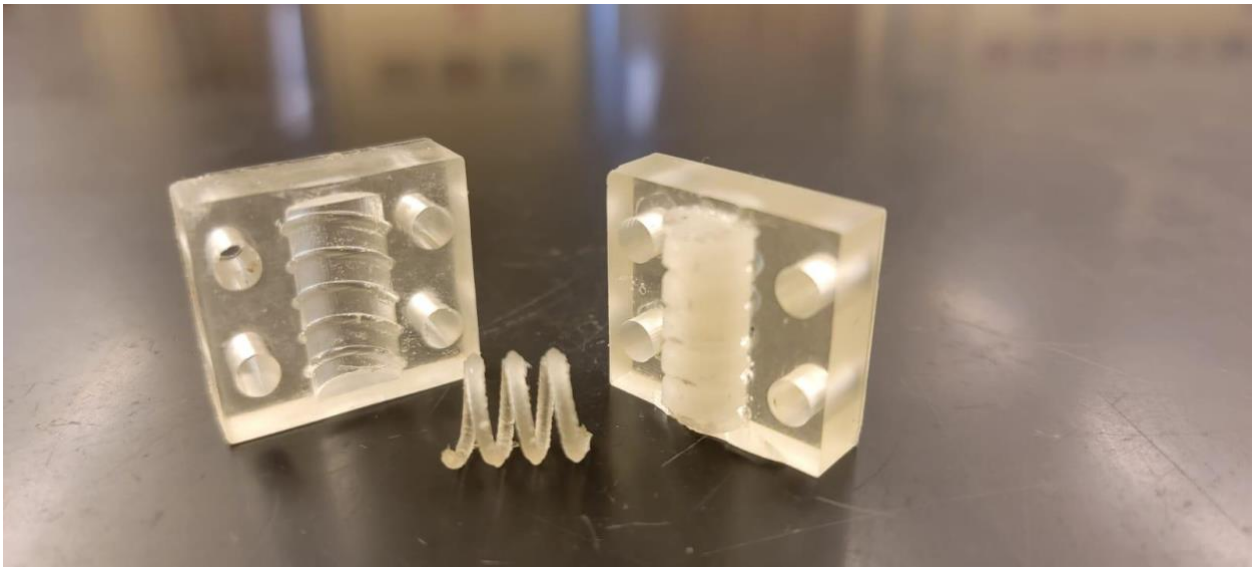

Figure 7 Fully cured spring after UV curing alongside the disassembled mold

2.2.2 Development of Nanocomposite Encapsulation:

The functional material in this design is a conductive nanocomposite. This nanocomposite is thermoplastic polyurethane (TPU) is a matrix with a carbon conductive material.

TPU is dissolved into Dimethylformamide (DMF) through magnetic hot stirring. Magnetic stirring is done for 40 minutes at 160 degrees.

In the meantime, graphene or CNTs are dissolved into DMF through sonication. An ice bath setup is prepared for the Carbon/DMF mix. Sonication is using sound energy to disperse the carbon particles into the solution by mobilizing the carbon particles. As sonication goes on, temperature increases. The temperature increase is caused by the sound energy and the agitation of carbon particles into the DMF solution. This temperature increase causes CNTs to clot and enhances the Van Der Waals forces among the carbon particles. here comes the significance of the ice bath as it keeps the mix at a cool temperature to prevent clotting. As the mix is kept cool the Van Der Waal forces' energy is kept at a minimum which makes

dispersion easier. As sonication is applied, energy from sonic waves is travels hrough the mix which increases the collisions among the particles in the solution which increases the overall temperature of the mix. Carbon is sonicated for 15 minutes in total on time. The on-time is the active time of sonication while the off-time is the time when the solution is at rest with no sonication. For carbon dispersion in DMF, the on-time was 3 seconds, and the off-time was 7 seconds. The probe sonicator used was Branson Sonifier SFX250 for which the amplitude is set as a percentage at 50% which equals an amplitude of 80 um.

After the carbon is sonicated into DMF, TPU-DMF, and Carbon-DMF are mixed. The carbon polymer matrix is created through hot plate stirring of both TPU in DMF and Carbon in DMF for 85 mins at 160 °C. Stirring is done at 160 °C which is higher than the DMF evaporation point to remove DMF.

The following images in figure 8 show the actual experimental setup for the sonication of MWCNTs in DMF with the application of an ice bath to minimize the temperature for better dispersion and less agglomeration of particles.

Figure 8 Sonication of MWCNTs in DMF within an ice bath

2.3 Spring coating process:

When the carbon/TPU composite is in a mushy state after hot stirring and removal of DMF, the spring is covered in the mushy mix to create the outer functional layer. The spring is rested in the mix for 1 minute and then hung for another 1 minute to drop any access material. The coated spring is then placed into the furnace for 2 hours at 160 °C to remove any remaining DMF and solidify the outer layer. Thermal treatment was examined for different durations with increments of 15 minutes, and it was concluded that 2 hours optimized the adhesion between layers and the mechanical behavior of the spring sensor. The resulting outer layer thickness (Carbon/ TPU) is around 150 µm.

Figure 9 Fully functional Spring Sensor after coating and thermal treatment

2.4 Characterization of spring response:

A special setup was created for the testing and characterization of the spring. Spring is placed between two probes to measure the resistivity of the spring against length. Spring resistivity is first measured in a natural relaxed state. The spring is then stretched by fixed increments of 2 mm and the corresponding resistivity is recorded.

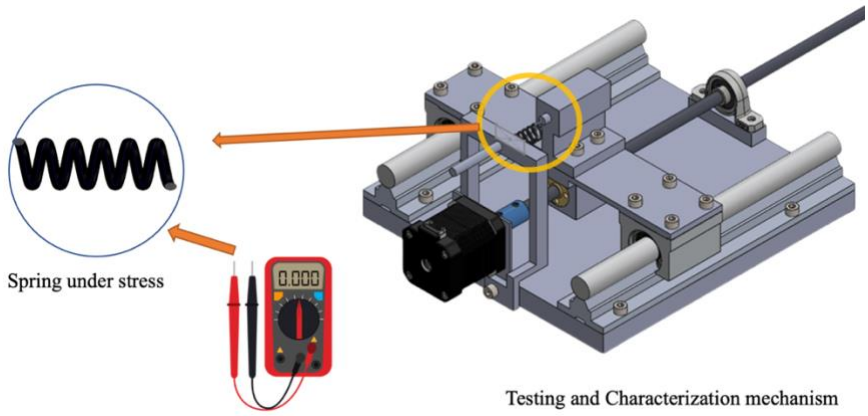

Figure 10 illustration of the sensor characterization assembly

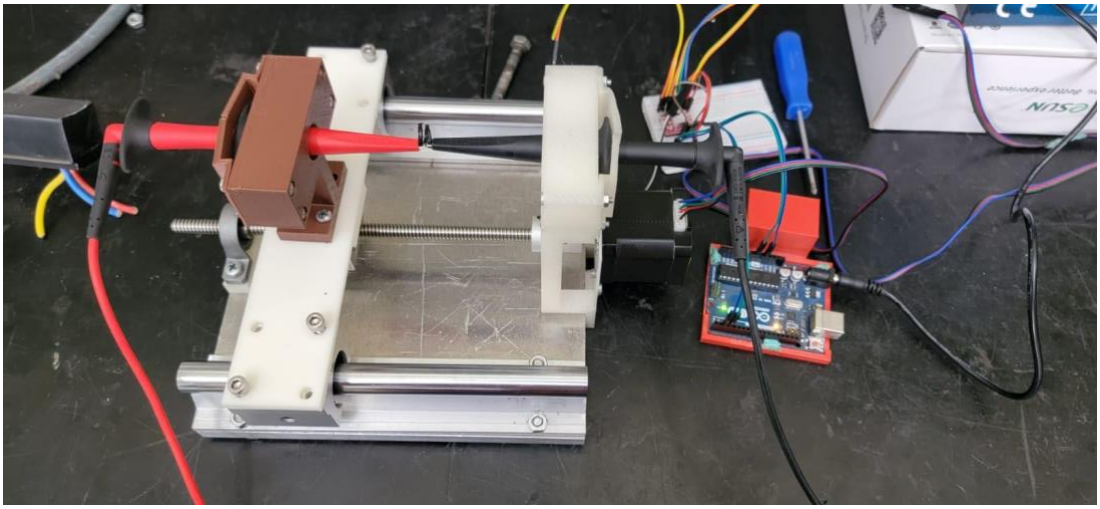

Figure 11 photograph of the actual characterization setup

2.5 Overall System Review:

The following diagram summarizes the overall fabrication processes employed in spring fabrication, development of the nanocomposite encapsulation, and integration of both to form the functional spring sensor.

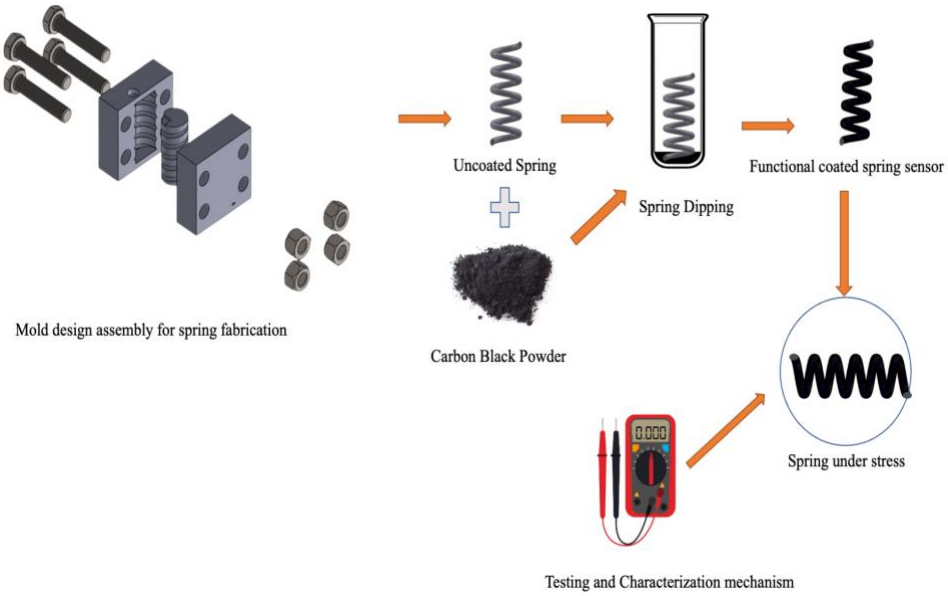

Figure 12 overview of the overall system processes in succession

Chapter 3

3. Results and Discussion

3.1 Morphological Characterization

Scanning electron microscope (SEM) was employed to study the morphology and filler dispersion of carbon into TPU. Cross section and the surface of 20% TPU/CB is characterized using Neoscope JCM-6000 plus-JEOL Benchtop SEM with magnifications ranging between X200 to X2000. As shown in Fig. 4 & Fig. 5, SEM characterization shows a high level of dispersion with a low degree of aggregation. Low aggregation means there is a better network established for electron tunneling which enhances the quality of the output signal by allowing better electron movement.

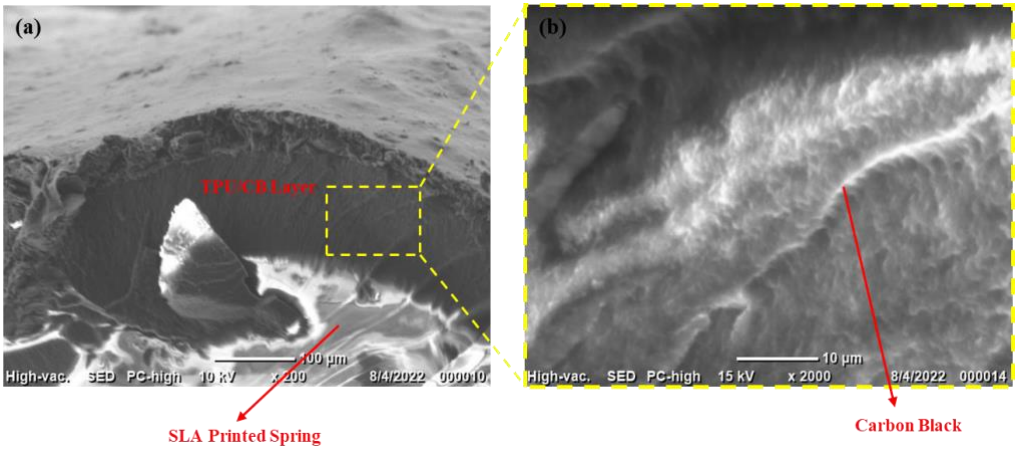

Figure 13 SEM image of the TPU/CB cross section, (a) Shows the SLA printed spring and the TPU/CB coating layer, (b) zoomed in image showing Carbon black dispersion in the TPU matrix.

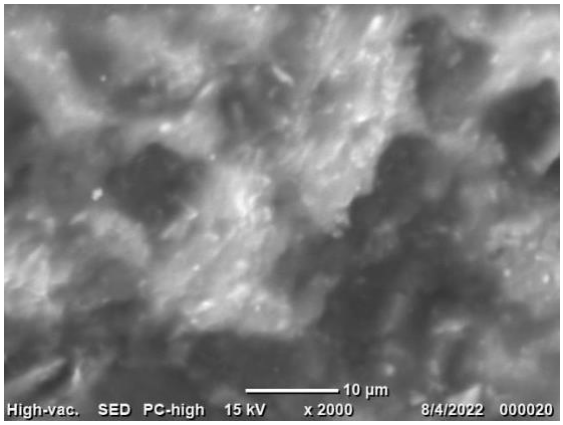

Figure 14 SEM image showing dispersion of carbon black on the surface of the TPU/CB coating,

3.2 Spring Sensor Characterization Results

Linear Deflection was applied on the TPU/CB springs while recording the resistances of the whole spring in parallel, to build a relation between extension and electronic properties, then an extension is translated to torsional strain recalling equation (8)

$$\gamma = \frac{\tau}{G} = \frac{8*W*D*K*\delta}{G*\pi*d^3} \qquad (8)$$

Where, γ is the torsional strain, W is Wahl's correction factor, D is the outer diameter of the spring, K is the stiffness, δ is the linear deflection, G is the shear modulus, and d is the spring diameter.

The following table summarizes the mechanical properties of the spring sensor to be used for characterization.

G (PLA-like material) (Mpa)	207
Spring wire section diameter (mm)	1.5
Spring wire section+ coating diameter (mm)	1.65
Spring Diameter	10

Number of Revolutions	2
K (spring stiffness) before coating	.065496
K (spring stiffness) after coating	.095892

Table 6 Dimensions and Properties of Characterized springs

Starting initial and final lengths are fixated for the consistency of measurements, with consistent deflection of δ = 2 mms. L initial = 6 mm and L final = 24 mm with the number of revolutions N= 2.

Recalling equations from the previous chapter and working with the values in table 5, the following derivation is done to calculate the corresponding torsional strain when the spring is stretched. This torsional strain will be reported with a change in resistivity to assess the electromechanical behavior of the springs.

$$G = \frac{E}{2 * (1 + \upsilon)}$$

$$G = \frac{538.2188}{2 * (1 + 0.3)} = 207\ MPa$$

$$K = \frac{d^4 * G}{8 *\ D^3 * N}$$

$$K_{before\ coating} = \frac{1.5^4 * 207}{8 *\ 10^3 * 2} = 0.065496094 \frac{N}{mm}$$

$$K_{after\ coating} = \frac{1.65^4 * 207}{8 *\ 10^3 * 2} = 0.095892831 \frac{N}{mm}$$

$$C = \frac{D}{d}$$

$$C = \frac{10}{1.5} = 6.667$$

$$W = \frac{4C - 1}{4C - 4} + \frac{0.615}{C}$$

$$W = \frac{(4 * 6.667) - 1}{(4 * 6.667) - 4} + \frac{0.615}{6.667} = 1.2246$$

$$\gamma = \frac{\tau}{G} = \frac{8 * W * D * K * \delta}{G * \pi * d^3}$$

$$\gamma = \frac{\tau}{G} = \frac{8 * 1.2246 * 10 * 0.04366 * \delta}{207 * \pi * 1.5^3} = 0.0019488\ \delta$$

Thus, by substituting the values for the extension applied to the spring δ, the corresponding value for torsional strain is obtained. δ is applied with consistent increments of 2 mm throughout all the experiments for the sake of consistency and accuracy of the results. It was shown by results and morphological characterization that as the spring is deflected, torsional strain is generated over the cross section of the spring, allowing the TPU/CB coating to relatively strain causing the distances between CB flakes to increase, decreasing the electron tunneling effect, which results in a dramatic increase in resistivity.

3.2.1 Multi-Walled Carbon nanotubes

This section summarizes the results of different composition percentages of the TPU polymer with Multi-Walled Carbon Nanotubes (TPU/MWCNTs) in the nanocomposite encapsulation. For each composition, the experiment was repeated a minimum of 3 times, for each experiment, 3 springs were produced and characterized to ensure the accuracy and reliability of the results. For each spring the strain/resistance results were recorded 3 times and the average was tabulated and then reported in the coming plots.

A linear regression model is fit onto the data to calculate the gauge factor of each spring at each composition. The slope of this linear regression model represents the relative change in resistance per strain applied. Therefore, the slope term represents the gauge factor for the spring sensor. For GF calculation, torsional strain is examined and not longitudinal strain because the longitudinal strain is affected by spring geometry such as initial length, pitch, and number of revolutions which varies among different springs. Therefore, results are more consistent with torsional strain. In the calculation of $\boldsymbol{\Delta R/R}$, the values for resistance are recorded 3 times and the average is used to calculate $\boldsymbol{\Delta R/R}$. However, longitudinal strain

results are documented for a better understanding of the electromechanical behavior of the tested spring sensors.

3.75 % MWCNTs

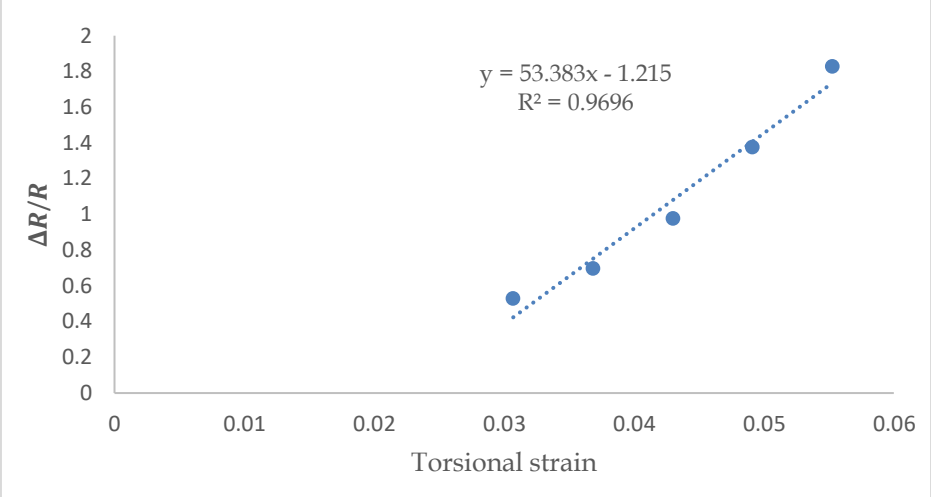

Figure 15 Spring 1 with 3.75 % MWCNTs in TPU

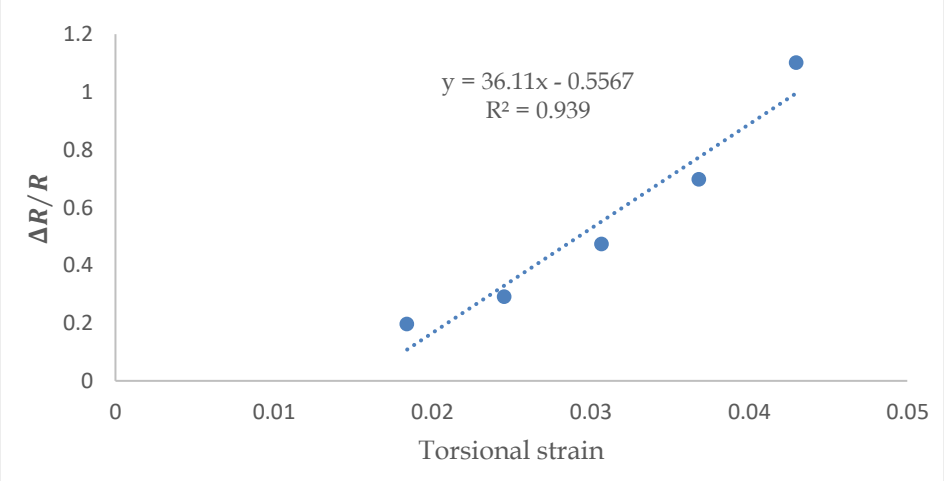

Figure 16 Spring 2 with 3.75 % MWCNTs in TPU

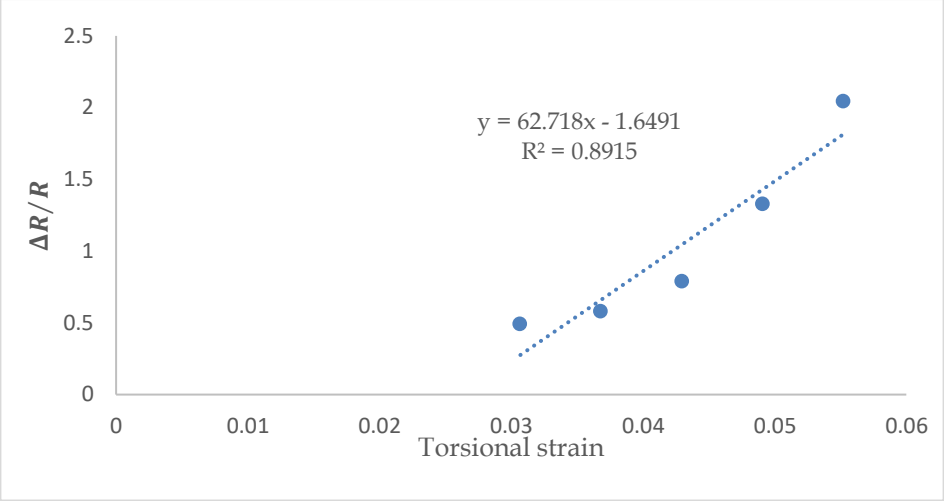

Figure 17 Spring 3 with 3.75 % MWCNTs in TPU

Sensors with 3.75% MWCNTs composition showed an adequate response with recorded GFs of 53.38, 36.1 and 62.7 which are low compared to GFs of composition around the percolation threshold of CNTs in TPU which will be evident in the coming reported results. Initially, when the strain is not significant the resistance change is not significant which is a problem that could be handled through pre-straining the sensor to avoid the steep linear region at the start.

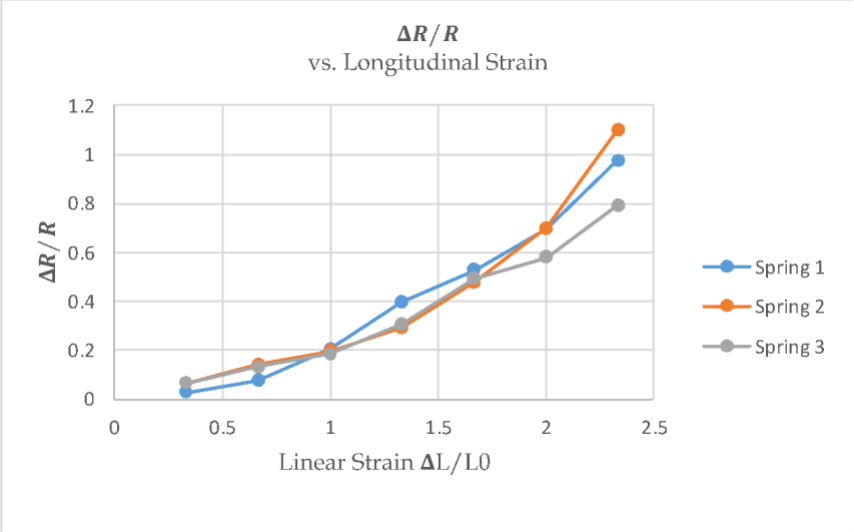

Figure 18 $\Delta R/R$ vs. Longitudinal Strain behavior for sensors with 3.75% MWCNTs composition

The behavior of the 3 springs shows similarity which indicates consistency in carbon dispersion in TPU and consistent mechanical behavior which validates the fabrication processes and their parameters.

4.25 % MWCNTs

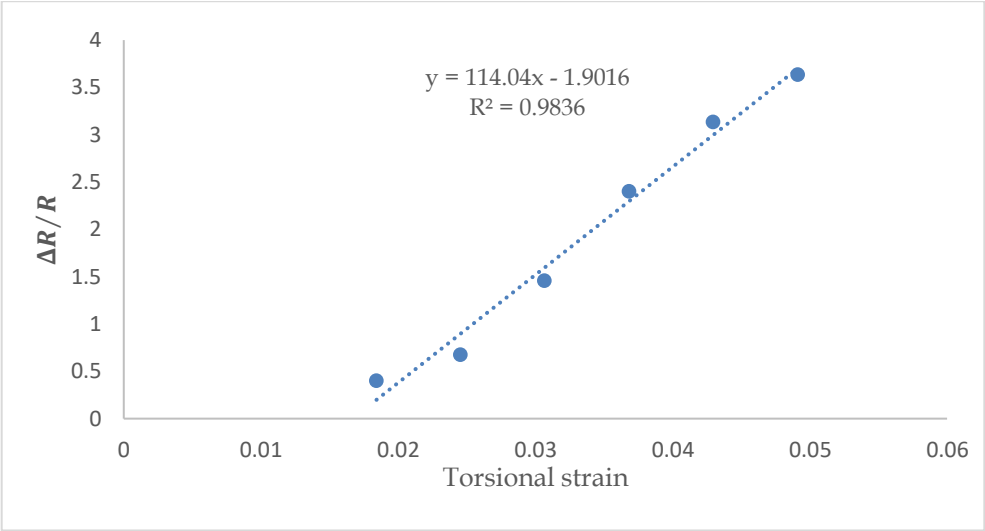

Figure 19 Spring 1 with 4.25% MWCNTs in TPU

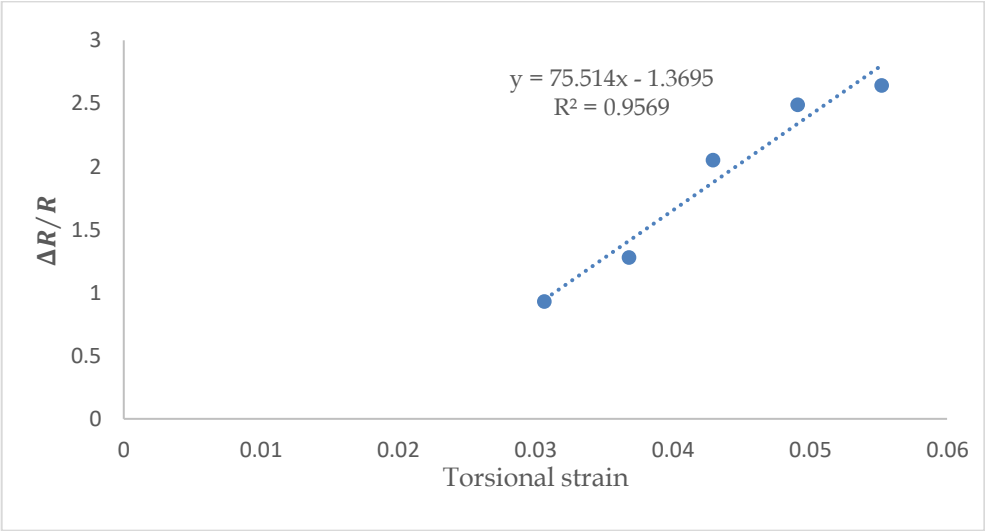

Figure 20 Spring 2 with 4.25% MWCNTs in TPU

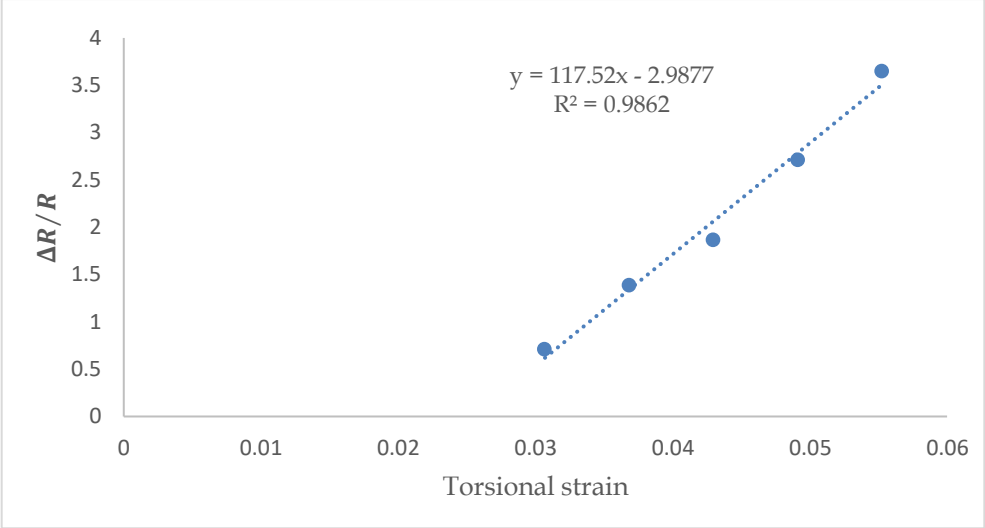

Figure 21 Spring 3 with 4.25% MWCNTs in TPU

As the percentage of CNTs increases in TPU, there is more conductivity and a possibility of electron tunneling occurring throughout the encapsulating layer. As strain increases, there is less possibility for electron tunneling and less potential for the presence of random connecting paths. At this composition, the TPU layer is sufficiently saturated with CNTs which is within the percolation threshold. At this point, the change in resistance is significant due to the strain which is reflected in the highest GF values for all CNT sensors.

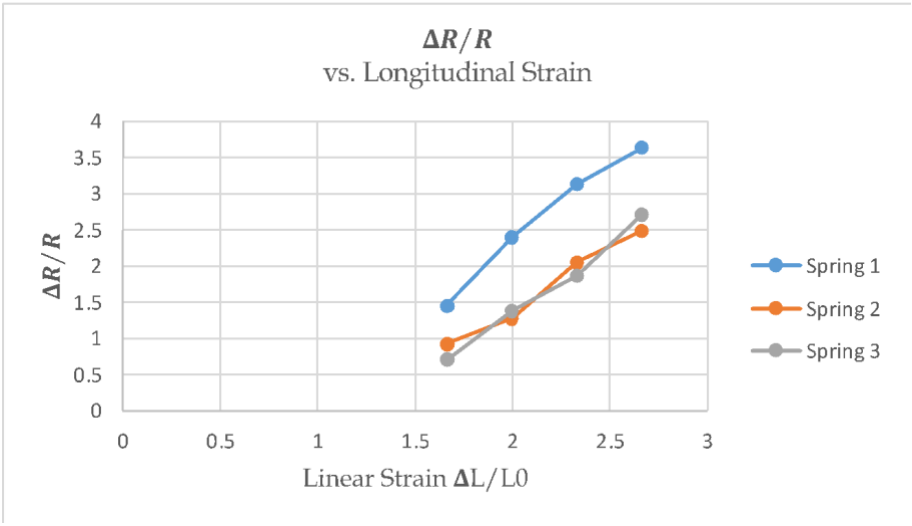

Figure 22 $\Delta R/R$ vs. Longitudinal Strain behavior for sensors with 4.25% MWCNTs composition

4.75 % MWCNTs

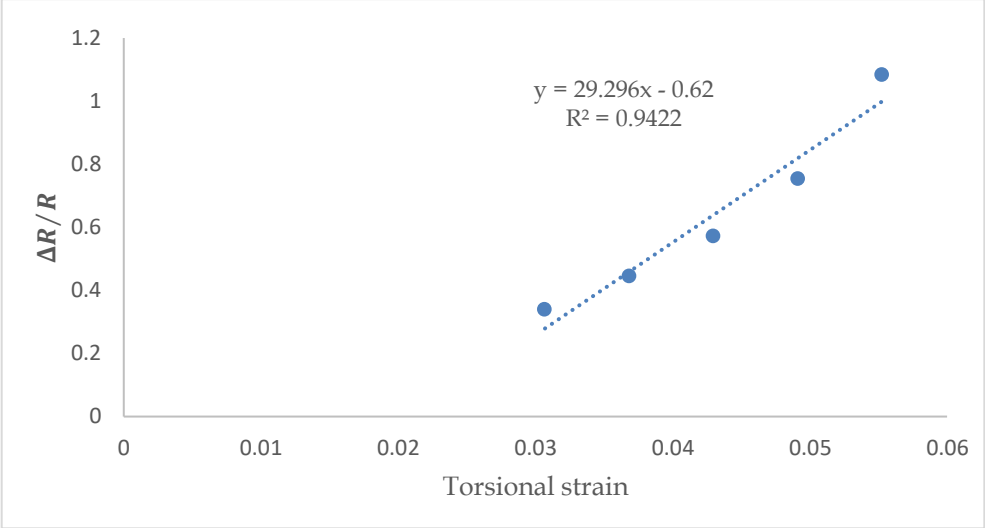

Figure 23 spring 1 with 4.75% MWCNTs in TPU

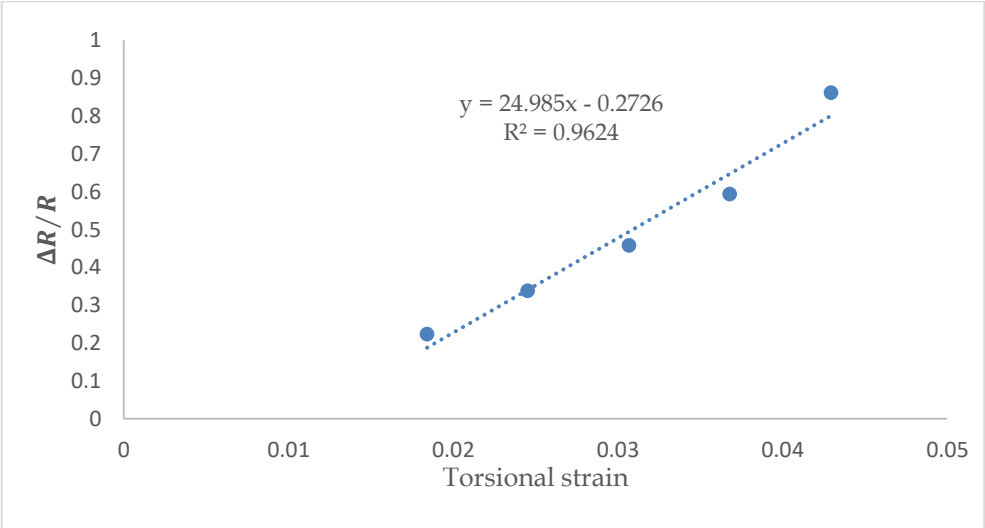

Figure 24 spring 2 with 4.75% MWCNTs in TPU

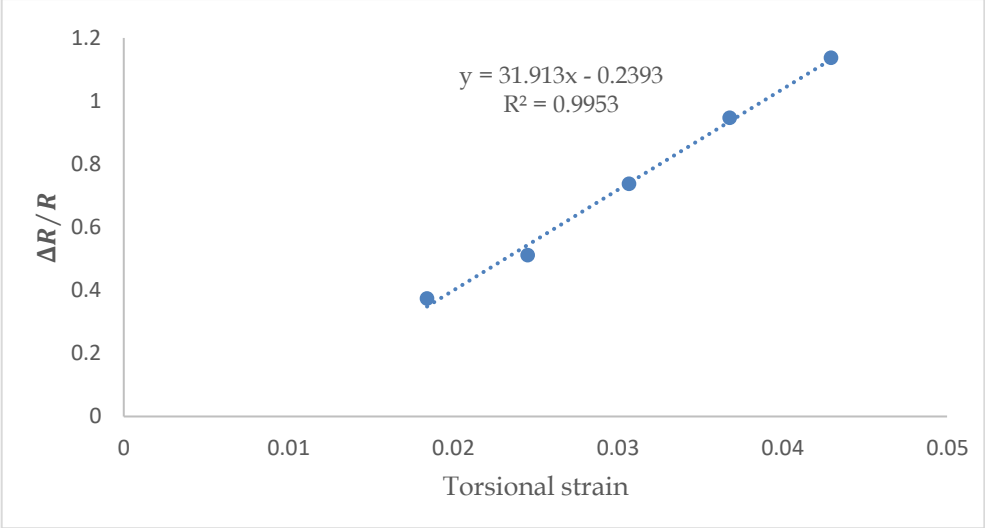

Figure 25 spring 3 with 4.75% MWCNTs in TPU

As the weight percentage composition of CNTs in TPU increases, there are way more random connective paths throughout the layer and easier conditions for tunneling and electron flow. this is evident in the low resistivity levels. This low resistivity is now less affected by the applied strain as electrons could find new shorter random paths as the orientation of conductive carbon particles changes. This is due to the presence of CNTs in abundance with this high composition beyond the percolation threshold range. Thus, change in resistivity is not significant with strain applied, leading to lower GF.

Moreover, to verify that CNT composition is now beyond the percolation threshold, the coming results are reported for the higher CNT composition. If the composition is beyond the threshold, it is expected that resistivity will decrease with lower dependency on the strain, accordingly lower GF.

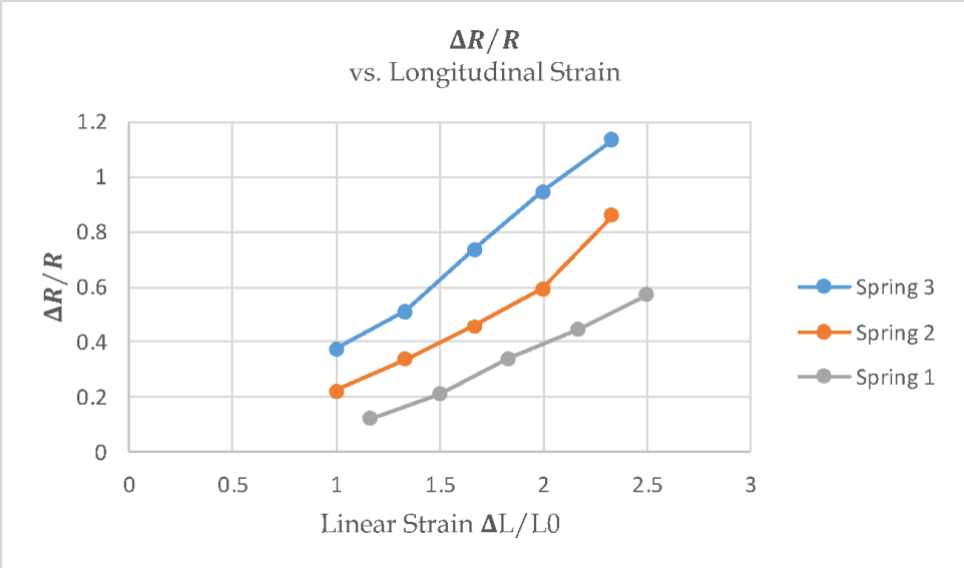

Figure 26 $\boldsymbol{\Delta R/R}$ vs. Longitudinal Strain behavior for sensors with 4.75 % MWCNTs composition

A noticeable variation is present in spring electronic behavior which could be attributed to the initial resistance value. This means that dispersion is varied across all three experiments leading to different initial R values at the same carbon weight percentage in TPU.

5.25 % MWCNTs

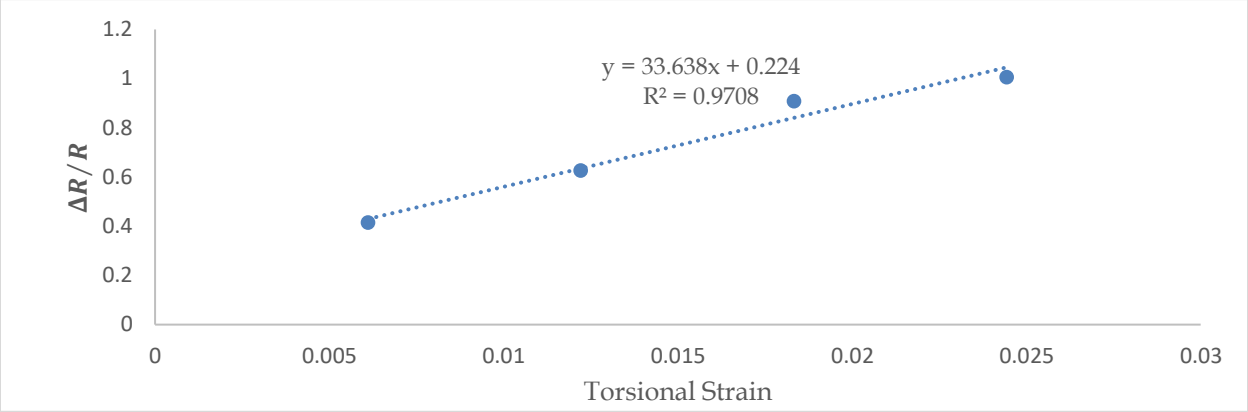

Figure 27 Spring 1 with 5.25% MWCNTs in TPU

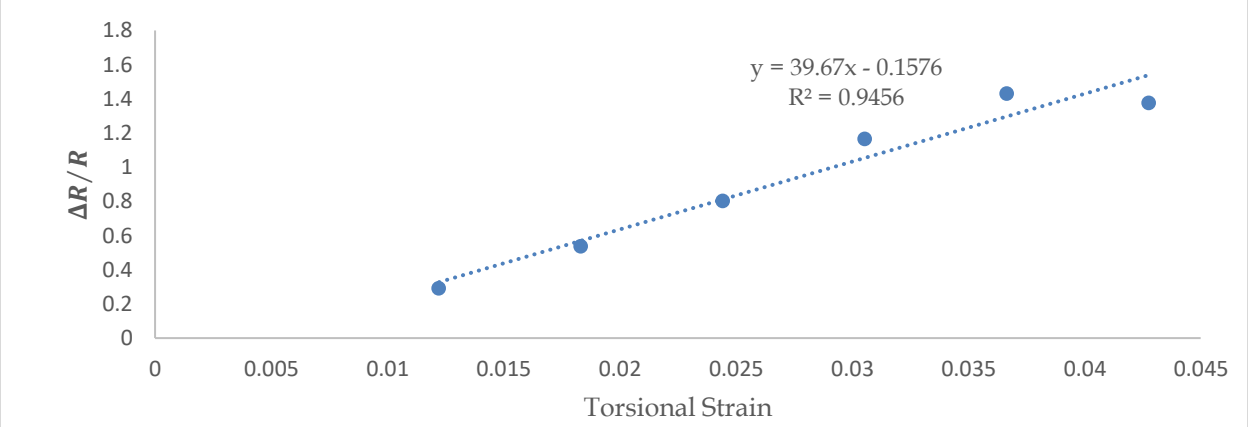

Figure 28 Spring 2 with 5.25% MWCNTs in TPU

As previously reported, the GF started to decrease dramatically as the CNT composition increased which decreases resistivity and how resistivity is sensitive to strain. For spring 1, more resistance ratio points are measured against torsional strain starting at 0 to see how the pre-straining effects works in this case. In the case of spring 1, the pre-straining effect is removed while spring 2 is pre-strained. As the percentage of MWCNTs increased, the matrix is now more conductive which is evident in the absence of a pre-strained effect which was evident in the other percentages. Spring 2 was pre-strained which resulted in a value near to spring 1 for

the GF which confirms that now at this percentage the spring is structure is super conductive which decreases the tunneling effects. Having now seen the results of the 5.25% composition, the percentage is now confirmed beyond the percolation threshold.

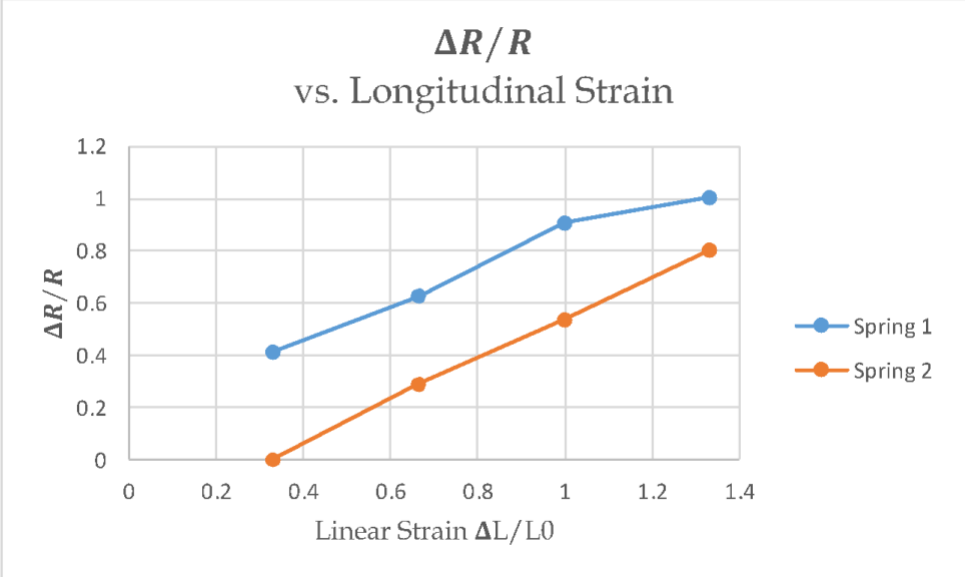

Figure 29 $\boldsymbol{\Delta R/R}$ vs. Longitudinal Strain behavior for sensors with 5.25% MWCNTs composition

MWCNTs Results Summary:

Figure 26 shows a summary of the average GF obtained for each experiment at each TPU-CNT composition.

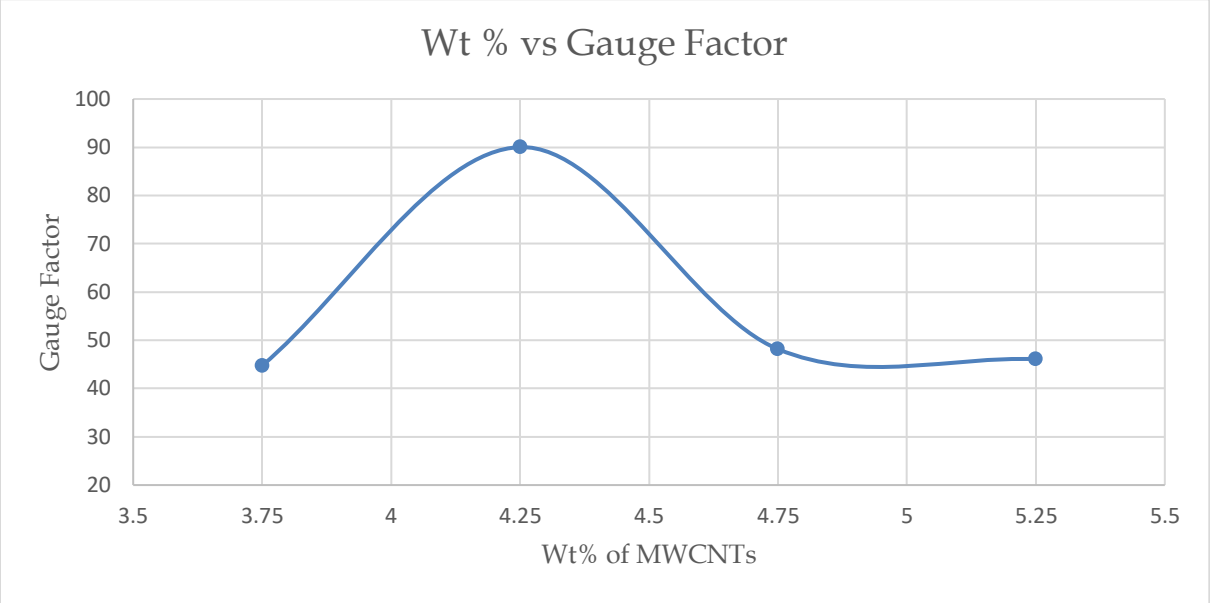

Figure 30 Summary of different CNT weight percentages in TPU Vs the corresponding Gauge Factor

The effect of the percolation threshold on the sensor's GF is now evident. Around the percolation range, resistivity is more sensitive to the strain applied which could provide better accuracy of strain measurements in different applications. the percolation threshold of MWCNTs in TPU is around 4.25% of the weight percentage.

The following figure 31 illustrates the average GF obtained for each composition with the standard deviation represented in the bar chart to better understand how severe the fluctuations of GF values are.

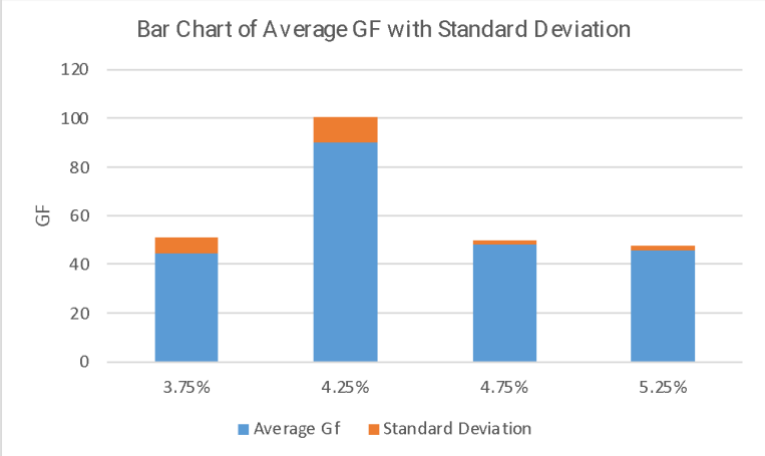

Figure 31 Bar chart for GF factor with standard deviation for all MWCNTs compositions in TPU

3.2.2 Graphene

this section summarizes the results of 4 different Graphene compositions starting a with 3.75% weight percentage.

3.75 % Graphene

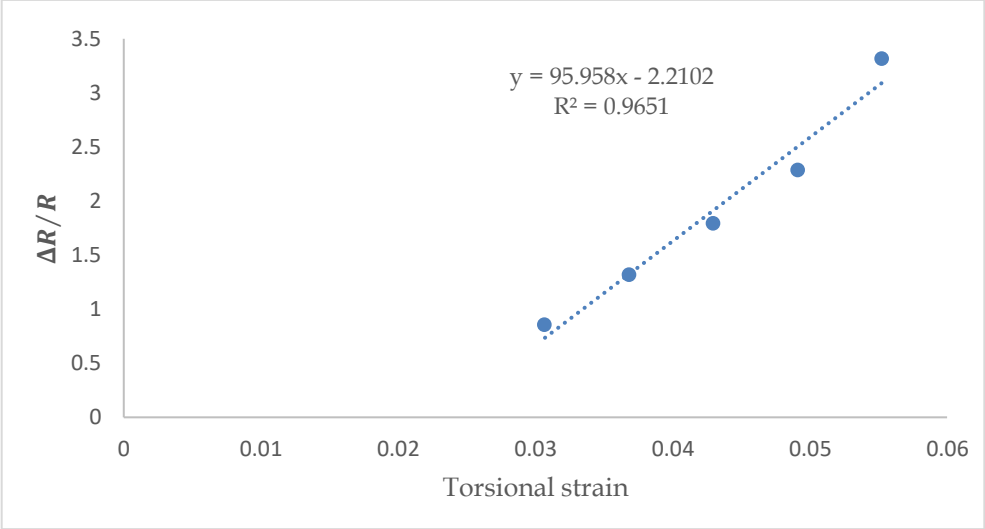

Figure 32 Spring 1 with 3.75% Graphene in TPU

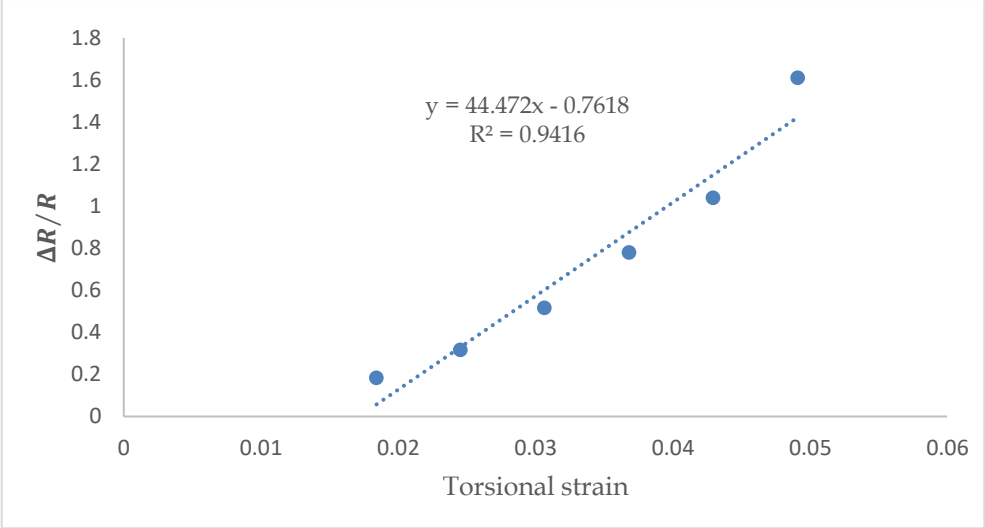

Figure 33 Spring 2 with 3.75% Graphene in TPU

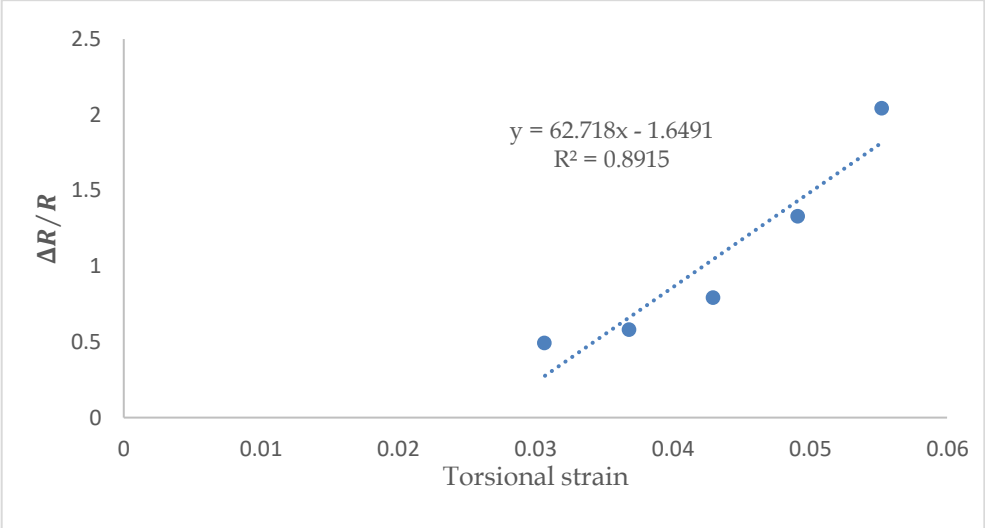

Figure 34 Spring 3 with 3.75% Graphene in TPU

Springs with 3.75% composition of graphene shows the variance in the GF values. This variation could be explained by agglomeration of graphene particles in the TPU matrix. Since graphene particles are larger compared to CNTs, it is most likely that graphene will agglomerate during the mixing process.

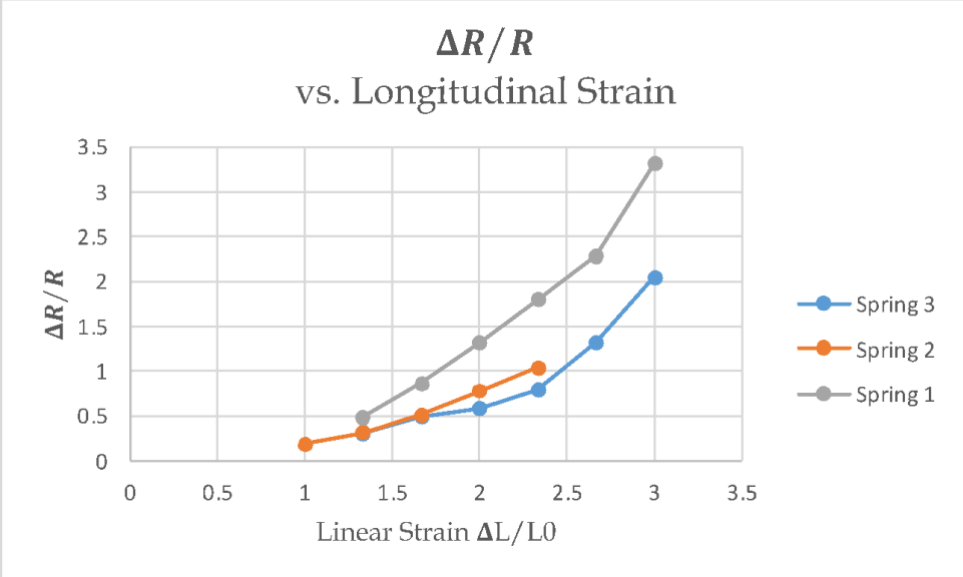

Figure 35 $\boldsymbol{\Delta R/R}$ vs. Longitudinal Strain behavior for sensors with 3.75 % Graphene composition

A more exponential trend is noticed in figure 35 which confirms the electromechanical behavior obtained from torsional strain and validates that 3.75% is within the percolation threshold.

4.25 % Graphene

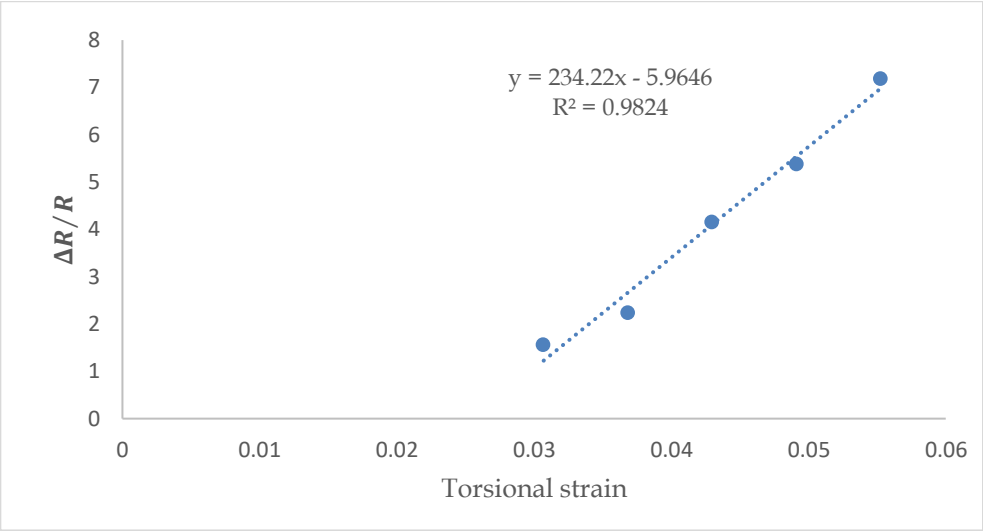

Figure 36 Spring 1 with 4.25 % Graphene in TPU

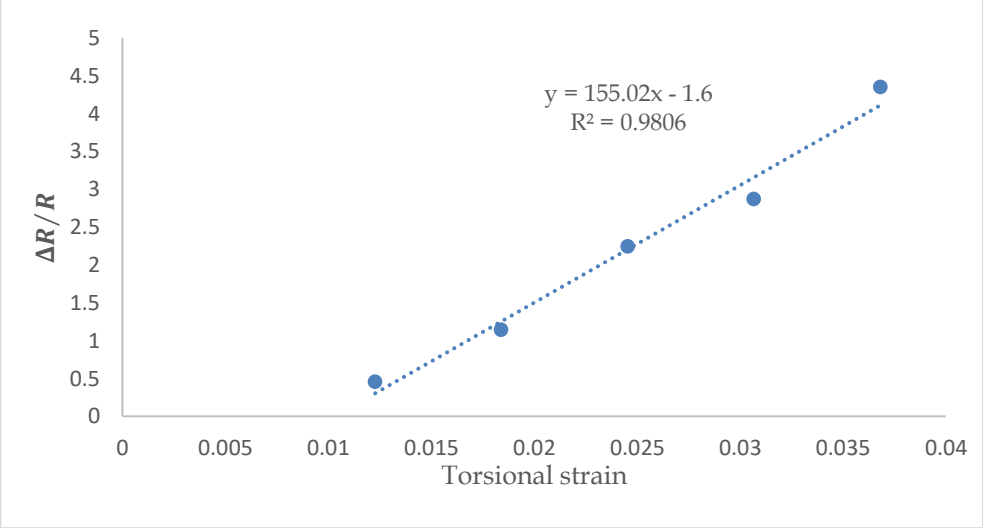

Figure 37 Spring 2 with 4.25 % Graphene in TPU

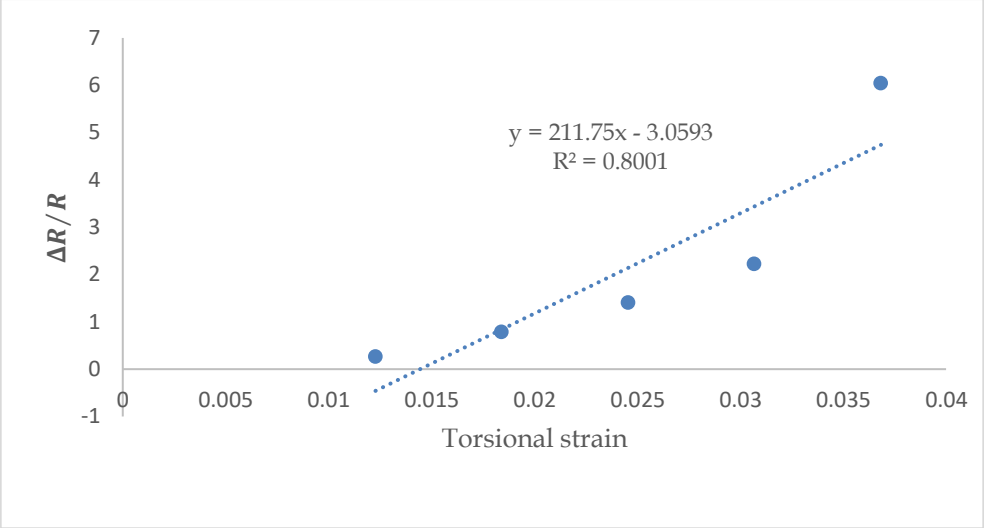

Figure 38 Spring 3 with 4.25 % Graphene in TPU

With 4.25% graphene in TPU, the results are becoming more consistent with two experiments resulting in GF above 200. While one experiment resulted in a GF of 155. The causes of variation in the process will further be analyzed in the coming discussion section. However, compared to values reported in the literature GF>200 is a great step forward.

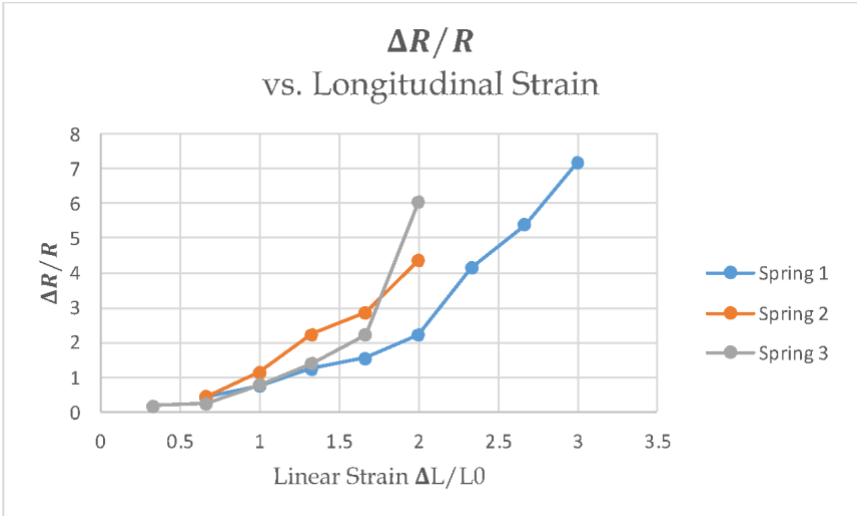

Figure 39 $\Delta R/R$ vs. Longitudinal Strain behavior for sensors with 4.25 % Graphene composition

The exponential trend is becoming clearer as the composition of graphene increases in TPU nearing the optimal value for percolation threshold.

4.75 % Graphene

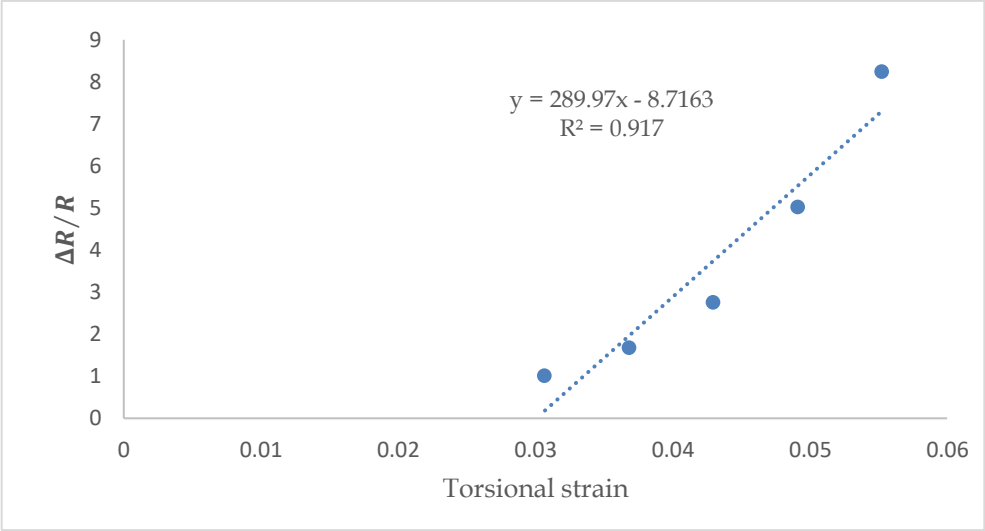

Figure 40 Spring 1 with 4.75 % Graphene in TPU

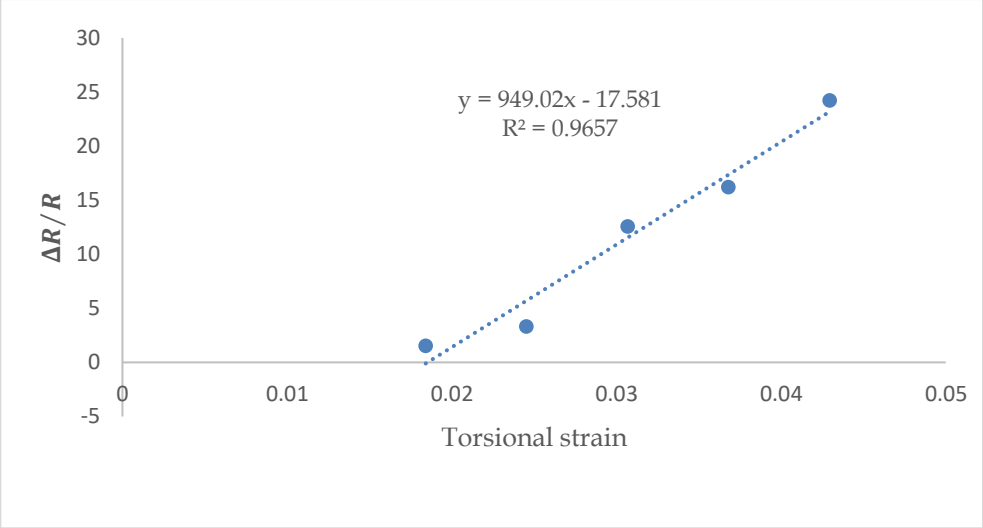

Figure 41 Spring 2 with 4.75 % Graphene in TPU

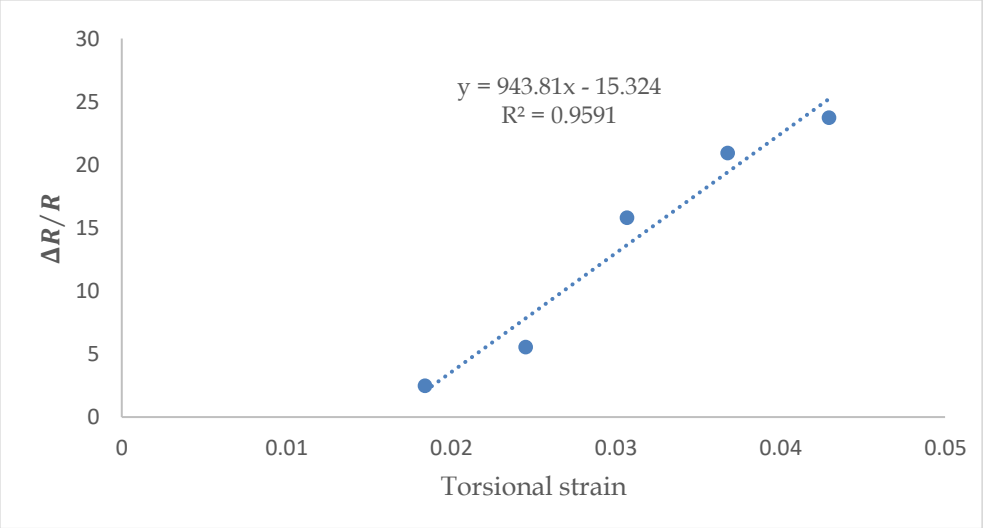

Figure 42 Spring 3 with 4.75 % Graphene in TPU

With 4.75% composition, spring sensors have shown great results with two experiments resulting in GFs 943.8 and 949. This significant increase in GF means this composition is now in the percolation threshold for graphene in TPU. To verify that, another weight percentage composition is done at 5.25% graphene.

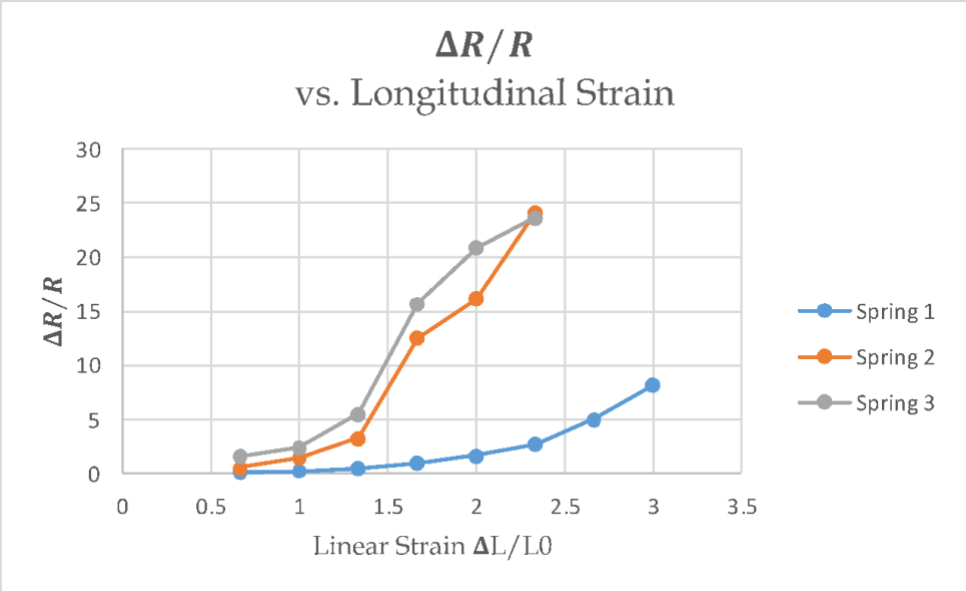

Figure 43 $\Delta R/R$ vs. Longitudinal Strain behavior for sensors with 4.75 % Graphene composition

The exponential trend is now at the peak as the composition of graphene in TPU is at the optimum percolation threshold confirming that small changes in linear strain and torsional strain result in a dramatic decrease in the tunneling effect among the dispersed graphene particles.

5.25 % Graphene

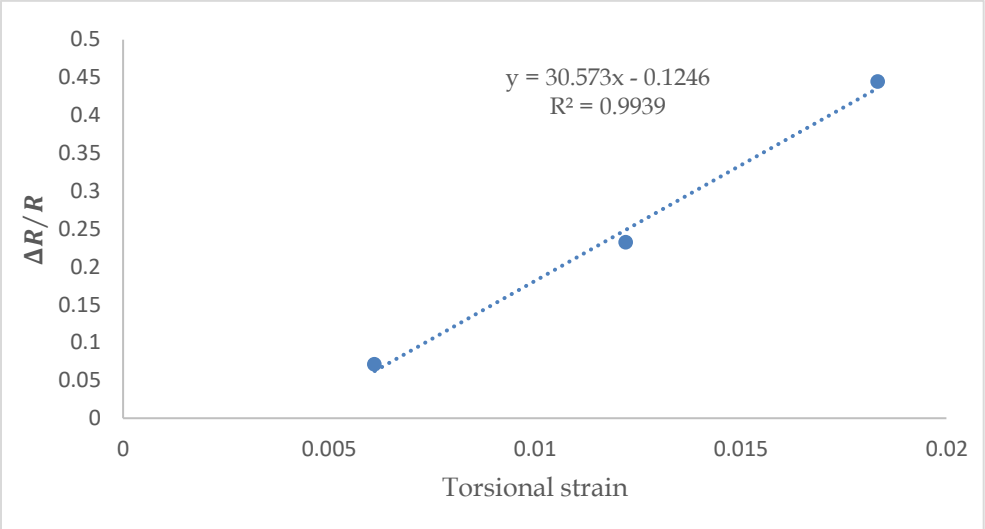

Figure 44 Spring 1 with 5.25 % Graphene in TPU

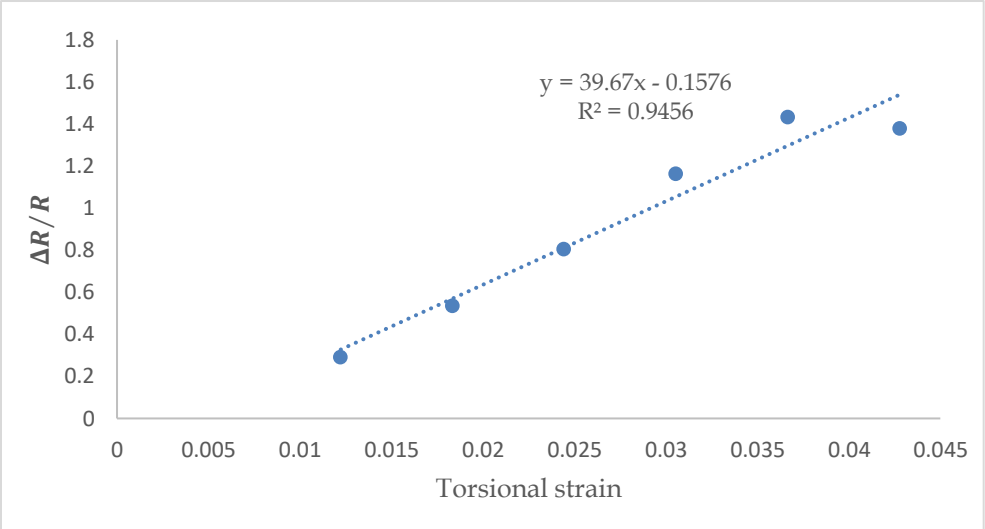

Figure 45 Spring 2 with 5.25 % Graphene in TPU

This 5.25% shows drastically lower GF compared to 4.75 % which verifies that this composition is high beyond percolation threshold. This is explained by lower resistivity due to increasing the conductive graphene content. GF decreases as resistivity is less sensitive to changes in strain applied.

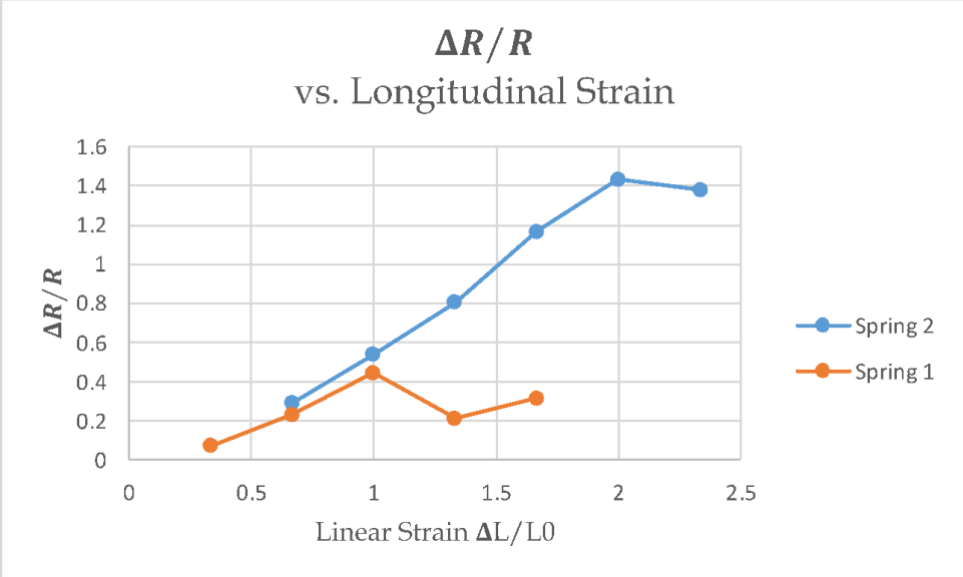

Figure 46 $\Delta R/R$ vs. Longitudinal Strain behavior for sensors with 5.25 % Graphene composition

As the composition of graphene exceeds the percolation threshold, exponential dependency decays and it is evident from figure 46 that it is beyond the percolation threshold as the composite is more conductive with less dependence on the linear or torsional strain.

Graphene Results summarized

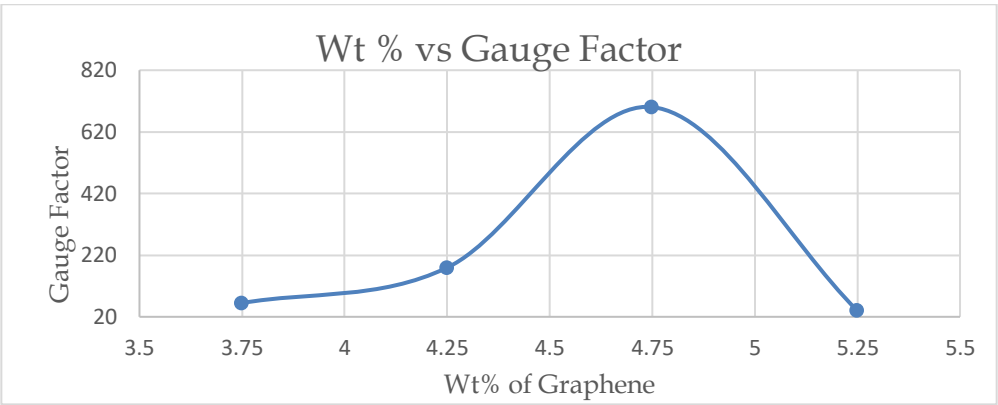

Figure 47 Summary of different Graphene weight percentages in TPU Vs the corresponding Gauge Factor

This summarizing plot shows that 4.75% graphene in TPU is the optimal percolation point with this percolation threshold reaching an average GF = 700 and maximum GF of 940.

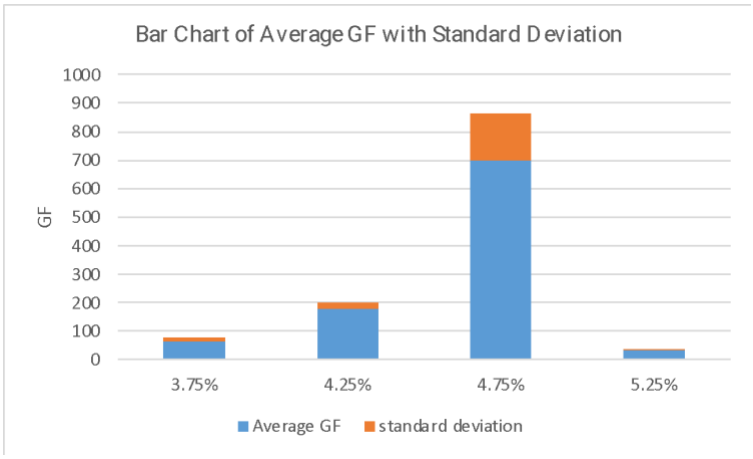

Figure 48 Bar chart for GF factor with standard deviation for all Graphene compositions in TPU

Real time respiration cycle simulation:

A simulation of the respiration cycle is done through the characterization assembly. The spring is continuously strained and relaxed to simulate the breathing mechanism. The following graph demonstrate the results of real-time monitoring using the spring sensor. One breathing cycle is simulated by a deflection of 8 mm in the spring with a duration of 6 seconds.

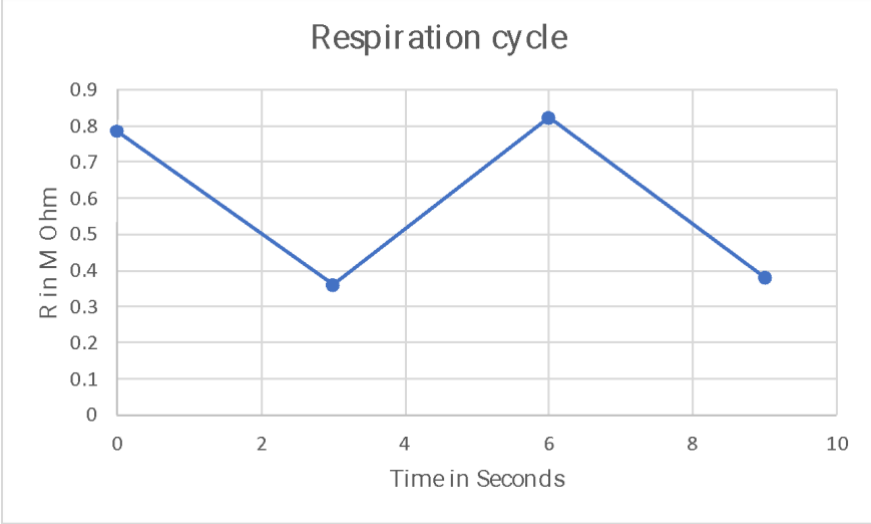

Figure 49 Respiration Cycle monitoring with a pre-strained sensor

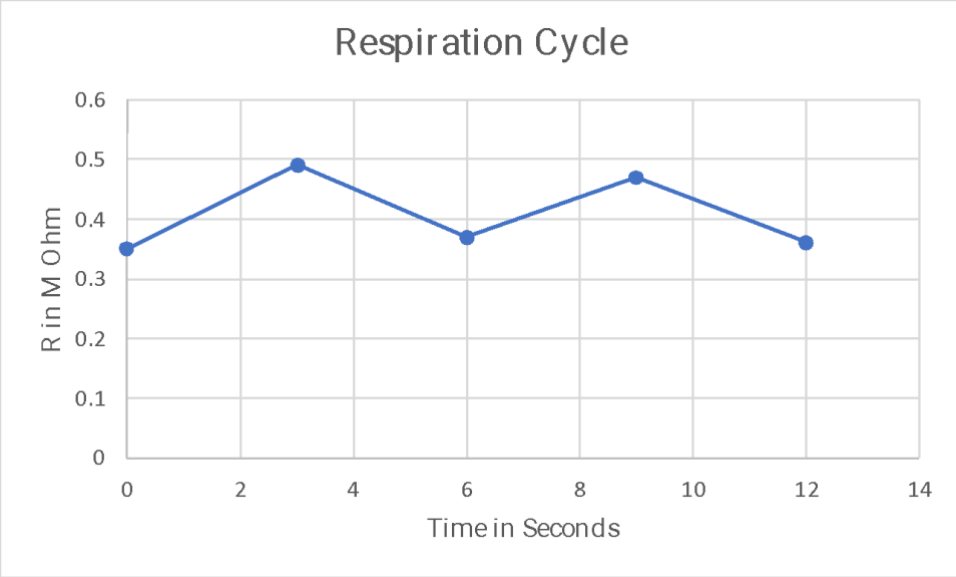

Figure 50 Respiration Cycle monitoring with a relaxed sensor

Breathing simulation applied to the spring sensor at real time breathing frequency near to 30 breaths/minute. The following figure demonstrates the results over 30 seconds.

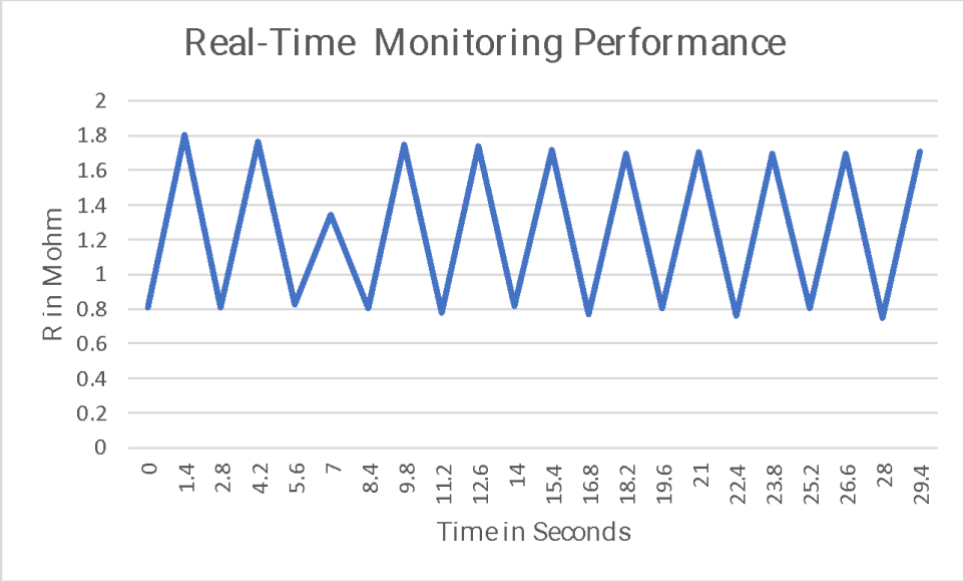

Figure 51 high frequency simulation of normal breathing pattern

The sensor was tested for continuous 12 hours to examine durability and consistency in the results over longer periods. Results were recorded on an hourly basis. There are some

fluctuations in the maximum R values recorded which could be attributed to the slip of the testing probe when fully extended at high frequency.

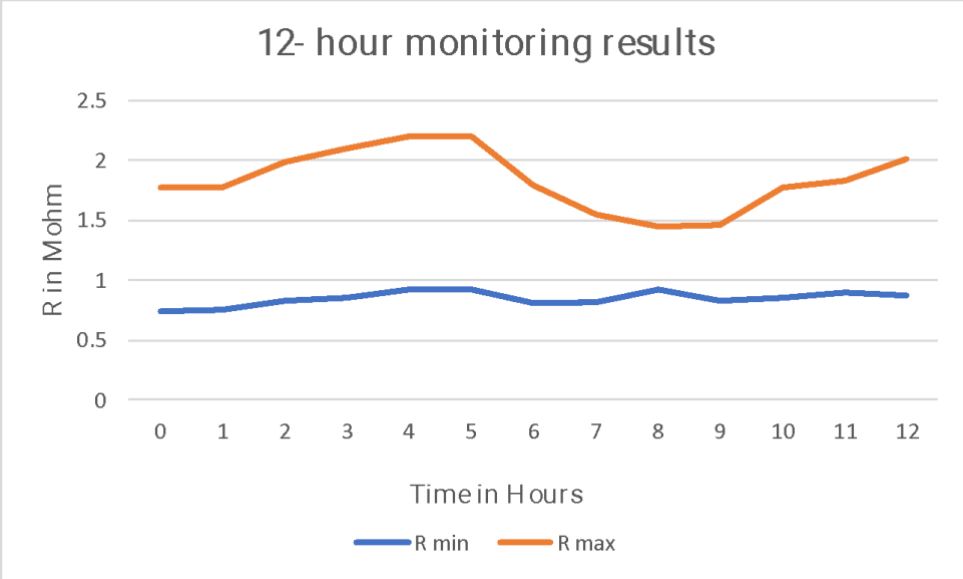

Figure 52 results of hourly monitoring of sensor response over 12 hours

3.3 Discussion

Device performance is analyzed and tested for two filler or functional materials: Multi-Walled Carbon Nanotubes and Graphene in TPU polymer. The Gauge Factor is reported for both materials and different compositions. The novel sensor design recorded a significant extension percentage reaching around 300%. MWCNTs in TPU produce optimal Gf at around 4.25% weight. Graphene in TPU is optimal at 4.75 % weight. These results are consistent with the literature are CNTs provide better conductivity due to their physical properties. CNTs have a higher surface area, allowing for more potential for electron tunneling. Thus, the optimal composition is at a lower weight percentage compared to graphene. In addition, as the filler nanoparticles decrease in size, the percolation threshold tends to decrease.

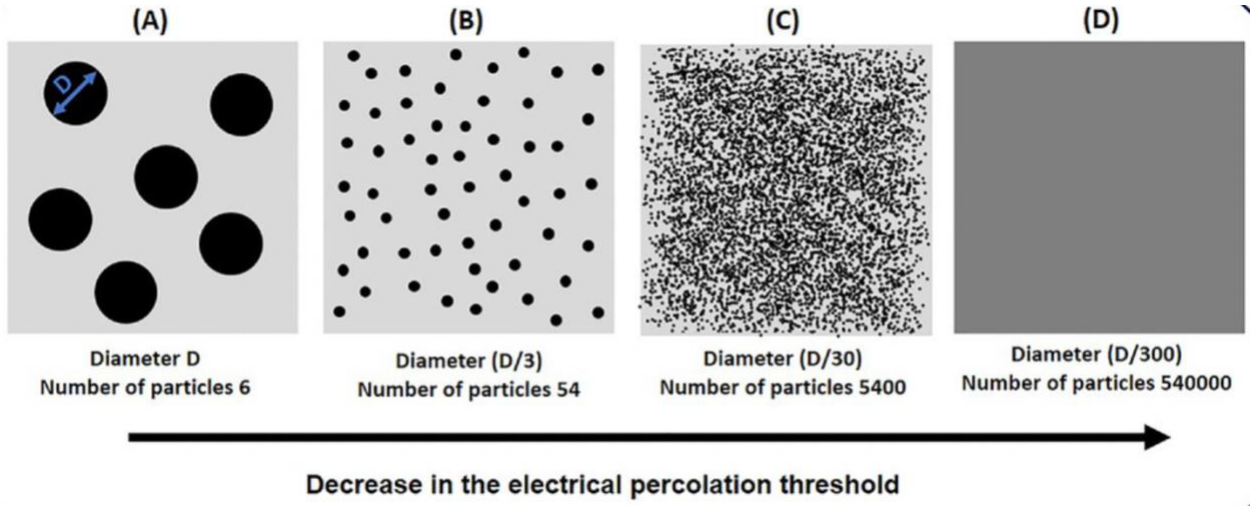

Figure 53 Percolation Threshold and Filler material particle size [32]

Variation in results could be attributed to numerous reasons. Human error plays a factor specially that the experimental procedure involved multiple processes. Outliers in the results are a few examples and could be caused by multiple reasons. Contamination of the experimental apparatus could fail the experiment. Furthermore, inconsistencies in the filler

material itself (CNT or Graphene) could cause this variation in the results. Since the coating technique is dipping, there could be some variation in the encapsulation layer thickness which affects the device's performance. In addition, a possible source of error is in the mixing temperature and sonication. Sonication causes high temperatures which might agglomerate the carbon particles together. The mixing process could cause variation due to some irregularities in the temperature of the magnetic stirrer. To overcome the possible causes of error, the experiments were repeated many times with consistency in the procedure to minimize the variation. Other sources of error could be in the spring itself (PLA-like material), the spring properties could be affected by variations in injection time, mold quality, and post-injection processes (thermal treatment and ultraviolet curing). These variations could affect the spring's mechanical properties due to irregularities in the spring's cross-section or the presence of air bubbles. As a result, it affects the spring stretchability, adhesion with encapsulating layer, and the overall response to applied strain.
Future work could be done to improve dispersion and interface interaction between MWCNTs and TPU through the functionalization of CNTs which will boost dispersion and lower the tendency of agglomeration which yields better interface interaction, and mechanical and electrical properties.

3.4 Conclusion

A novel strain sensor is introduced consisting of a PLA-Like Spring encapsulated with a TPU/Carbon functional composite. This project aimed at optimization of the spring design, material selection, fabrication processes, and fine-tuning the composition of the TPU/Carbon layer to yield maximum gauge factor and extension for the spring. The strain applied to this spring sensor changes the resistivity as electron tunneling behavior changes within the percolation threshold.

The proposed work targets shortcomings in literature in the field of respiration monitoring systems which include the following:

- Textile sensors as wearable respiration monitoring systems have low reported gauge factors
- Reliability of the results are vulnerable to local changes in skin perfusion with possibilities of causing skin irritation.

Employing the novel strain sensor addresses the abovementioned shortcomings

- The spring sensor provides great stretchability.
- High Gauge Factors result in higher sensitivity and better accuracy.

Application of this novel spring design has reported the following key findings:

- Extension within the elastic region reaching around 300% of the spring's original length at rest.
- The optimized TPU/Graphene composition within the percolation threshold is at 4.75% weight percent of graphene in TPU resulting in a gauge factor of 950.
- The optimized TPU/MWCNT composition within the percolation threshold is at 4.25% weight percent of CNTs in TPU resulting in a gauge factor of 117.

Furthermore, this project optimized the fabrication techniques for spring sensor development which are:

- For spring fabrication: starting with mold 3d-printing via stereolithography then injection molding (injection rate) of spring material followed by UV curing (exposure time) and thermal treatment for optimal mechanical behavior.
- For Encapsulation nanocomposite layer fabrication: sonication (amplitude, duration, and on/off time), magnetic hot plate stirring (temperature and duration) for dispersion of carbon particles in TPU for enhanced electronic

properties.

In addition to process optimization, composition optimization is critical for spring behavior. Fine-tuning the filler carbon material composition within the percolation threshold was successfully done through multiple iterations to reach the ultimate composition. This fine-tuning resulted in enhanced electronic properties.

Optimized material composition and fabrication techniques through iterative processes yield great electromechanical properties which are evident in the consistency of results reported except for two outliers. This spring sensor has great mechanical and electrical properties that have great potential for various applications.

3.5 Future work:

Future work that could improve this work would target the following points:

- Since now the material composition is optimized the at the percolation threshold, future work could ensure uniform dispersion of carbon in the encapsulation layer.
- Improve the injection process to avoid air bubbles, and inconsistencies in the spring wire cross section that could cause stress concentrations.
- Exploring the behavior of functionalized carbon nanotubes as a filler for the nanocomposite
- Testing and characterization of fatigue performance of the sensor.

References

[1] Nag, Anindya, Roy BVB Simorangkir, Dinesh R. Gawade, Suresh Nuthalapati, John L. Buckley, Brendan O'Flynn, Mehmet Ercan Altinsoy, and Subhas Chandra Mukhopadhyay. "Graphene-based Wearable Temperature Sensors: A Review." *Materials & Design* (2022): 110971.

[2] Yang, Junliang, Kai Ling, Longhui Liu, Xianghui Zeng, Xiaowen Xu, Zheling Li, and Pei He. "Printable and Wearable Graphene-based Strain Sensor with High Sensitivity for Human Motion Monitoring." *IEEE Sensors Journal* (2022).

[3] Marjanovic, Nicolas, et al. "An Easy and Accurate Respiratory Rate Monitor Is Necessary." *Journal of Clinical Monitoring and Computing,* vol. 34, 2020.

[4] Chourpiliadis, Charilaos. "Physiology, Respiratory Rate." *National Library Of Medicine,* 2021.

[5] Nicolò, Andrea, et al. "The Importance of Respiratory Rate Monitoring: From Healthcare to Sport and Exercise." *Sensors*, vol. 20, no. 21, 2020, p. 6396., https://doi.org/10.3390/s20216396.

[6] Ali, Mohamed, et al. "Contact and Remote Breathing Rate Monitoring Techniques: A Review." *IEEE Sensors Journal*, vol. 21, no. 13, 2021, pp. 14569–14586., https://doi.org/10.1109/jsen.2021.3072607.

[7] Villegas, P. "Viral Diseases of the Respiratory System." *Poultry Science*, vol. 77, no. 8, 1998, pp. 1143–1145., https://doi.org/10.1093/ps/77.8.1143.

[8] Beck, Jennifer, et al. "Characterization of Neural Breathing Pattern in Spontaneously Breathing Preterm Infants." *Pediatric Research*, vol. 70, no. 6, 2011, pp. 607–613., https://doi.org/10.1203/pdr.0b013e318232100e.

[9] Meuret, Alicia E., et al. "Respiratory Feedback for Treating Panic Disorder." *Journal of Clinical Psychology*, vol. 60, no. 2, 2004, pp. 197–207., https://doi.org/10.1002/jclp.10245.

[10] Dieffenderfer, James, et al. "Low-Power Wearable Systems for Continuous Monitoring of Environment and Health for Chronic Respiratory Disease." *IEEE Journal of Biomedical and Health Informatics*, vol. 20, no. 5, 2016, pp. 1251–1264., https://doi.org/10.1109/jbhi.2016.2573286.

[11]Javanbakht, Mehdi, et al. "Continuous Monitoring of Respiratory Rate with Wearable Sensor in Patients Admitted to Hospital with Pneumonia Compared with Intermittent Nurse-Led Monitoring in the United Kingdom: A Cost-Utility Analysis." *PharmacoEconomics - Open*, vol. 6, no. 1, 2021, pp. 73–83., https://doi.org/10.1007/s41669-021-00290-7.

[12]Bandyopadhyay, Dhrubajyoti, et al. "Covid-19 Pandemic: Cardiovascular Complications and Future Implications." *American Journal of Cardiovascular Drugs*, vol. 20, no. 4, 2020, pp. 311–324., https://doi.org/10.1007/s40256-020-00420-2.

[13]R Burgos-Vargas. "Chest Expansion in Healthy Adolescents and Patients with the Seronegative Enthesopathy and Arthropathy Syndrome or Juvenile Ankylosing Spondylitis." *National Library of Medicine, National Center for Biotechnology Information,* 1993.

[14]Olsén, Monika Fagevik, et al. "Measuring Chest Expansion; a Study Comparing Two Different Instructions." *Advances in Physiotherapy*, vol. 13, no. 3, 2011, pp. 128–132., https://doi.org/10.3109/14038196.2011.604349.

[15]Merck & Co, Inc., "Diaphragm's role in breathing", MSD Manual. Rahway, NJ, USA

[16] Megan O'Reilly, Foula Sozo, Richard Harding,. "Impact of preterm birth and bronchopulmonary dysplasia on the developing lung: Long-term consequences for respiratory health". Clinical and experimental pharmacology and physiology, 2013 Vol 40, Issue 11, Pages 765-773

[17] Kevin Looia,et al. " Preterm birth: Born too soon for the developing airway epithelium?" Pediatric Respiratory Reviews, 2019. Volume 31, August 2019, Pages 82-88

[18] Leigh R. Sweet, et al. "Respiratory distress in the neonate: Case definition & guidelines for data collection, analysis, and presentation of maternal immunization safety data" National library of medicine, National center for biotechnology information. 2017

[19] David J. Gallacher, Kylie Hart, and Kotecha "Common respiratory conditions of the newborn". National library of medicine, National center for biotechnology information 2016 12(1): 30–42.

[20] Seung Hye Han and Rama K. Mallampalli "The Role of Surfactant in Lung Disease and Host Defense against Pulmonary Infections". National library of medicine, National center for biotechnology information 2015 May; 12(5): 765–774.

[21]Sudeep Yadav, Brian Lee, Ranjith Kamity "Neonatal Respiratory Distress Syndrome" Statpearls Publishing. 2022

[22]SS Mathai, U Raju, and M Kanitkar "Management of Respiratory Distress in the Newborn"2007 Medical Journal Armed Forces India 63(3): 269–272.

[23]Graeme R. Polglase, "Respiratory support for premature neonates in the delivery room: effects on cardiovascular function and the development of brain injury" Nature pediatric research, 2014

[24] Khaled A Abdel Baseer, Mostafa Mohamed, Eman A Abd-Elmawgood "Risk Factors of Respiratory Diseases Among Neonates in Neonatal Intensive Care Unit of Qena University Hospital, Egypt" Annals of Global Health. 2020

[25]Gabriel Beltrão, et al." Contactless radar-based breathing monitoring of premature infants in the neonatal intensive care unit". Nature. 2022

[26]Massaroni, C. et al. "Optoelectronic plethysmography in clinical practice and research: a review". *Respiration* **93**, 339–354 (2017).

[27] H. Ceren Ates, et al. "End-to-end design of wearable sensors". Nature Review Materials 887–907 (2022)

[28] Abdallah Kamal, et al. "Fabrication techniques of nanocomposites, a comprehensive", Journal of Mechanical Engineering Science. 2022 vol.236 (9)

[29]Zhou, Zhen, Shifeng Wang, Yong Zhang, and Yinxi Zhang. 2006. "Effect of Different Carbon Fillers on the Properties of PP Composites: Comparison of Carbon Black with Multiwalled Carbon Nanotubes." *Journal of Applied Polymer Science* 102 (5): 4823–30. https://doi.org/10.1002/app.24722.

[30]Balberg, I. 2002. "A Comprehensive Picture of the Electrical Phenomena in Carbon Black–Polymer Composites." *Carbon* 40 (2): 139–43. https://doi.org/10.1016/s0008-6223(01)00164-6.

[31]Kausar, Ayesha. 2018. "Contemporary Applications of Carbon Black-Filled Polymer Composites: An Overview of Essential Aspects." *Journal of Plastic Film & Sheeting* 34 (3): 256–99. https://doi.org/10.1177/8756087917725773.

[32] Lei, Hua, William G. Pitt, Lucas K. McGrath, and Clifford K. Ho. 2007. "Modeling Carbon-Black/Polymer Composite Sensors." Sensors and Actuators. B, Chemical 125 (2): 396–407. https://doi.org/10.1016/j.snb.2007.02.041.

[33] Spring Manufacturers Institute Inc. "Encyclopedia of Spring Design", 2000

[34] Spring Engineers "How To Design A Spring".

[35] https://www.mathworks.com/matlabcentral/fileexchange/64651-design-optimization-of-a-helical-compression-spring

[36] Leonardo de Souza Vieira, et al. "A review concerning the main factors that interfere in the electrical percolation threshold content of polymeric antistatic packaging with carbon fillers as antistatic agent" Nanoselect, 2022. Vol (3)

[37] T. Khan, et al. "Insights to low electrical percolation thresholds of carbon-based polypropylene nanocomposites" Carbon. 2021. Vol (176)